Supplementary Information (SI) for Inorganic Chemistry Frontiers.

Supporting Information

Anion-modulated photoswitching of a tetraurea-bridged azobenzene

Yue Wang [b], Yu Tao [c], Xu Lu [d], Chaochao Fan [e], Dan Zhang [c], Tian Wang [b], Shulei Feng [a], Wenyao Zhang [a*], Chuandong Jia [c*]

[a] *Key Laboratory of Magnetic Molecules and Magnetic Information Materials of Ministry of Education, School of Chemistry and Chemical Engineering, Shanxi Normal University, TaiYuan 030031, China*

[b] *Shaanxi Coal Based Special Fuel Research Institute Co., Ltd, Xi'an 710100, China*

[c] *Key Laboratory of Synthetic and Natural Functional Molecule of the Ministry of Education, College of Chemistry and Materials Science, Northwest University, Xi'an 710069, China*

[d] *Institute for Hygiene of Ordnance Industry, Xi'an 710065, China*

[e] *Shaanxi Key Laboratory of Comprehensive Utilization of Tailings Resources, College of Chemical Engineering and Modern Materials, Shangluo University, Shangluo 726000, China*

E-mail addresses: zhangwenyao@sxnu.edu.cn, jcd2015@nwu.edu.cn

TABLE Of CONTENTS

S1. General Considerations

o-Nitro-phenylisocyanate were purchased from Alfa Aesar and used as received. All solvents and other reagents were of reagent grade quality and purchased commercially. ^{1}H and ^{13}C NMR, and ^{1}H-^{1}H COSY spectra were recorded on a Bruker AvanceIII-400/600 and JNM-ECZ400S NMR spectrometer, at 400/600 and 100 MHz, using residual solvent peaks as the internal standard for the ^{1}H and ^{13}C spectral analyses. **L^{1}**-a and **L^{1}**-b were synthesized by previous methods.[1]

The mass spectra of ligand **L^{1}**, intermediates, and anion complexes were measured with a Bruker micrOTOF-Q II ESI-Q-TOF LC/MS/MS spectrometer. The samples were dissolved in acetonitrile and measured using the following ESI parameters: Spray voltage = 4.5 kV; dry gas at 8.0 l/min; temperature: 150 °C; collision energy: 2 eV; mass range: 500-3000 amu.

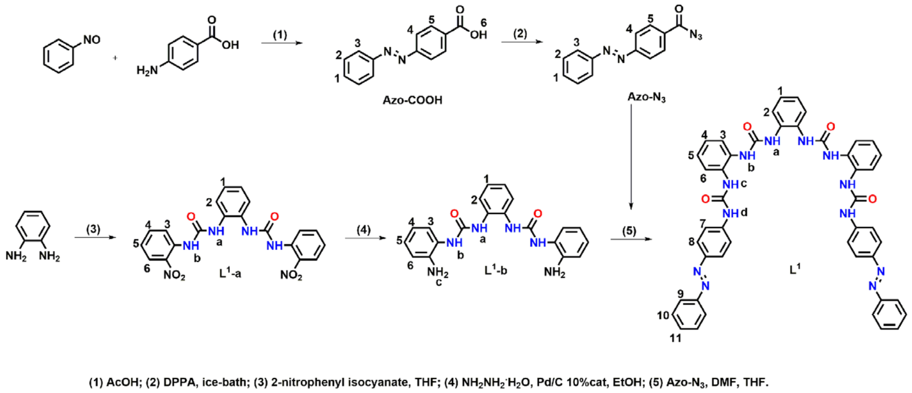

Scheme 1. Synthesis of ligand **L^{1}**

S2. Synthesis of Ligand L^{1}

Compound Azo-COOH

Nitrosamine benzene (2.00 g, 18.68 mmol) and *p*-aminobenzoic acid (3.08 g, 22.46 mmol) were dissolved in 30 mL glacial acetic acid. After stirring for 24 h under room temperature, the resulting precipitate was filtered off and washed several times with water, and purify by recrystallization with ethyl acetate to obtain pure product (Azo-COOH) as an orange solid (3.4 g, 15.05 mmol, 81 %). ^{1}H NMR (400 MHz, DMSO-d_6, ppm): δ 13.25 (s, 1H, H6), δ 8.16 (d, *J = 8.0 Hz*, 2H, H5), δ 7.89 (d, *J = 8.0 Hz*, 2H, H4), 7.95-7.93 (m, 2H, H3), 7.66-7.62 (m, 2H, H2/1). ^{13}C NMR (100 MHz, DMSO-d_6, ppm): *δ* 166.7 (CO), 154.3 (C), 151.9 (C), 132.9 (C), 132.2 (CH), 130.6 (CH), 139.6 (CH), 122.8 (CH), 122.6 (CH). ESI-MS: *m/z* 249.07 [M+Na]$^{+}$.

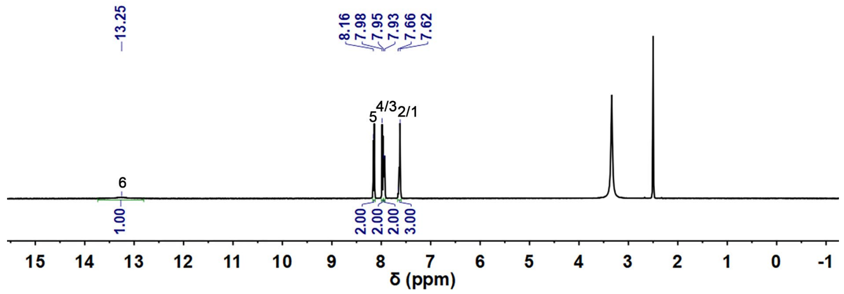

Fig S1. ^{1}H NMR spectrum of compound **Azo-COOH** (400 MHz, DMSO-d_6, 298 K).

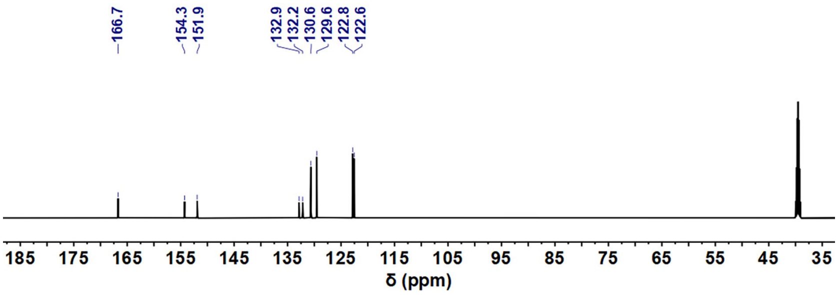

Fig S2. ^{13}C NMR spectrum of compound **Azo-COOH** (100 MHz, DMSO-d_6, 298 K).

Compound Azo-N$_3$

The compound **Azo-COOH** (1.00 g, 4.42 mmol) and triethylamine (1.4 mL) was added to a 20 mL THF solution, stirring until **Azo-COOH** dissolved. Under ice bath conditions, added diphenyl azide phosphate (DPPA, 2.2 mL, 6.26 mmol) and stirring at room temperature for 2 h. The solvent was removed, and crude product was extracted twice with DCM/H_2O, the organic phase was collected, and after drying with anhydrous sodium sulfate, the solvent was removed and obtain orange solid product **Azo-N$_3$ (**0.95 g, 3.78 mmol, 86 %**)**. ^{1}H NMR (400 MHz, DMSO-d_6, ppm): δ 8.18 (d, J = *8.0 Hz*, 2H, H5), 8.02 (d, J = *8.0 Hz*, 2H, H4), 7.96-7.94 (m, 2H, H3), 7.63 (t, 2H, H2/1). ^{13}C NMR (100 MHz, DMSO-d_6, ppm): δ 172.0 (CO), 156.0 (C), 152.6 (C), 132.0 (C), 130.6 (CH), 129.3 (CH), 123.3 (CH), 122.9 (CH). ESI-MS: m/z 274.07 [M+Na]$^+$.

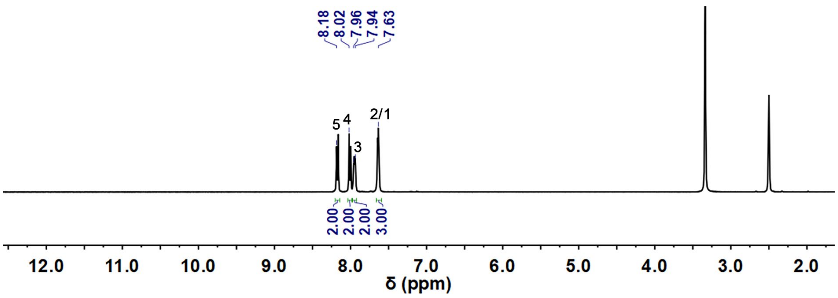

Fig S3. ^{1}H NMR spectrum of compound **Azo-N$_3$** (400 MHz, DMSO-d_6, 298 K).

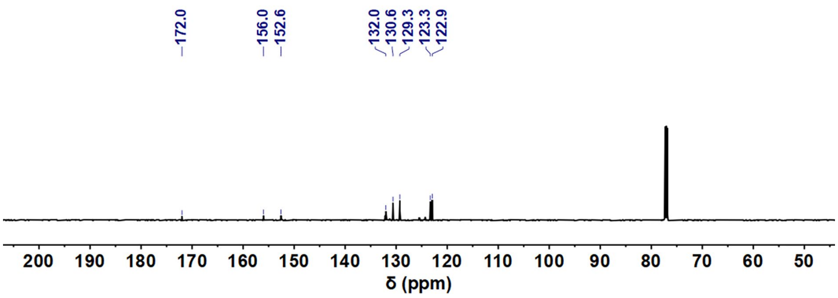

Fig S4. ^{13}C NMR spectrum of compound **Azo-N$_3$** (100 MHz, DMSO-d_6, 298 K).

L^1

Under nitrogen atmosphere, compound **L^1**-b (300 mg, 0.80 mmol) was dissolved in 3 mL DMF and 9 mL THF, and stirred at 60 °C for 10 min. Then, the compound **Azo-N$_3$** (445 mg, 1.75 mmol) was dissolved in 6 mL THF and dropped into the reaction flask. The temperature was raised at 80 °C and reacted for 24 h. After the reaction was completed, the reaction solution became clear. The THF and DMF were removed by rotary evaporation. A small amount of acetone was added to the concentrated solution and it sank into petroleum ether (30~60 °C), generating a large amount of orange precipitate. the resulting precipitate was filtered off and washed several times with 0.06 M HCl, water and acetone. It was then dried under vacuum to yield analytically pure ligand **L**[1] as an orange solid (542 mg, 0.66 mmol, 83 %).^{1}H NMR (400 MHz, DMSO-d_6, ppm): δ 9.57 (s, 1H, Hd), 8.54 (s, 1H, Hc), 8.50 (s, 1H, Hb), 8.21 (s, 1H, Ha), 7.84 (t, 4H, H7/8), 7.67-7.52 (m, 8H, H3/4/6/8/9/10/11), 7.10-7.07 (m, 3H, H1/2/5). ^{13}C NMR (100 MHz, DMSO-d_6, ppm): δ 154.2 (CO), 152.9 (CO), 152.1 (CO), 146.6 (CO), 143.3 (CH), 131.3 (CH), 131.2 (CH), 130.8 (CH), 124.3 (CH), 124.1 (CH), 123.9 (CH), 122.2 (CH), 118.1 (CH). ESI-MS: m/z 845.27 $[M+Na]^+$.

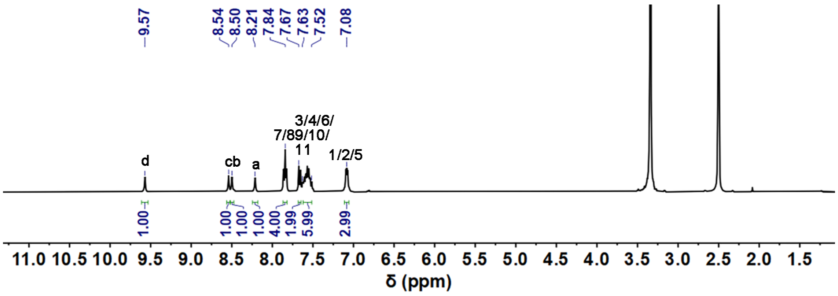

Fig S5. ^{1}H NMR spectrum of ligand **L**^{1} (400 MHz, DMSO-d_6, 298 K).

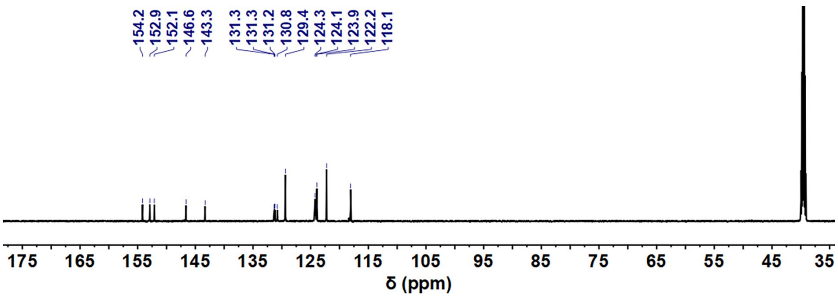

Fig S6. ^{13}C NMR spectrum of **L**^{1} (100 MHz, DMSO-d_6, 298 K).

S3. Synthesis of Anion Complexes

$(TMA)_3[(PO_4)]_1(\mathbf{L}^1)_2$ (complex *EE*-3)

$(TMA)_3PO_4$ (10 µL, 0.625 mol/L; generated *in situ* from TMAOH and H_3PO_4) was added to a suspension of **L**^{1} (10 mg, 12 mmol) in acetone (1 mL). After stirring overnight at room temperature, a clear orange solution was obtained. The clear solution was collected and poured into 10 mL diethyl ether. The precipitate thus obtained was filtered off, washed by 1 mL diethyl ether for three times, and dried over vacuum to give the product as an orange powder (yield > 90%). ^{1}H NMR (400 MHz, DMSO-d_6, ppm): δ 7.99 (d, 1H, H3), 7.81 (m, 3H, H2/8), 7.68 (d, 1H, H6), 7.55-7.48 (m, 5H, H7/9/11), 7.34 (s, 1H, H10), 7.02 (m, 2H, H4/5), 6.93 (t, 1H, H11).

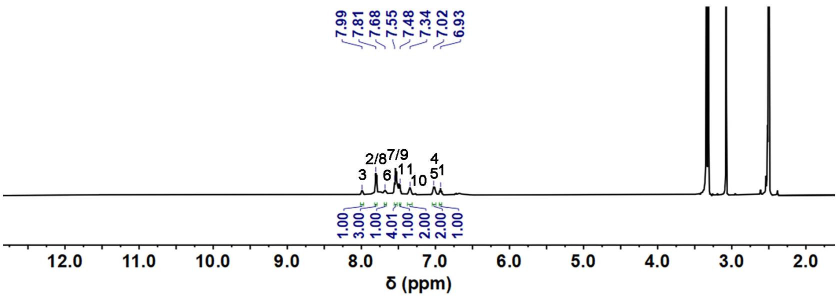

Fig S7. ^{1}H NMR spectrum of complex $(TMA)_3[(PO_4)]_1(\mathbf{L}^1)_2$ (***EE*-3**) (400 MHz, DMSO-d_6, 298 K).

$(TMA)_3[(PO_4)]_1(L^1)_1$ (complex *EE*-4)

$(TMA)_3PO_4$ (20 µL, 0.625 mol/L; generated *in situ* from TMAOH and H_3PO_4) was added to a suspension of **L**[1] (10 mg, 12 mmol) in acetone (1 mL). After stirring overnight at room temperature, a clear orange solution was obtained. The clear solution was collected and poured into 10 mL diethyl ether. The precipitate thus obtained was filtered off, washed by 1 mL diethyl ether for three times, and dried over vacuum to give the product as an orange powder (yield > 90%). ^{1}H NMR (400 MHz, DMSO-d_6, ppm): δ 7.98 (d, 1H, *J* = *8.0 Hz*, H3), 7.88 (d, 2H, *J* = *8.0 Hz*, H9), 7.83 (d, 2H, H2/6), 7.77 (d, 2H, *J* = *8.0 Hz*, H7), 7.54 (d, 2H, *J* = *8.0 Hz*, H8), 7.50 (t, 2H, H10), 7.43 (t, 1H, H11), 6.91 (t, 1H, H4), 6.87-6.83 (m, 2H, H1/5).

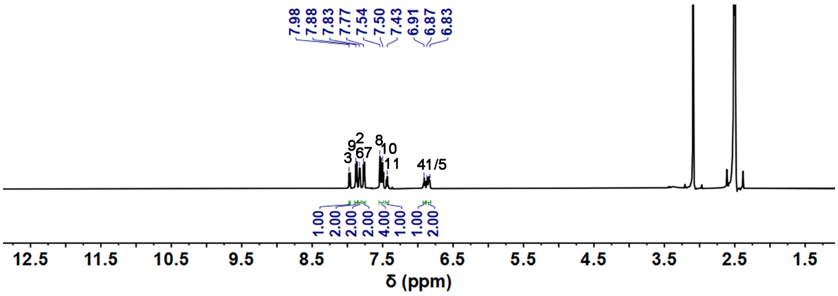

Fig S8. ^{1}H NMR spectrum of complex $(TMA)_3[(PO_4)]_1(\mathbf{L^1})_1$ (***EE*-4**) (400 MHz, DMSO-d_6, 298 K).

$(TMA)_2[(SO_4)]_1(L^1)_1$ (complex *EE*-5)

$(TMA)_2SO_4$ (10 µL, 0.625 mol/L; generated *in situ* from TMAOH and H_2SO_4) was added to a suspension of **L**[1] (5 mg, 6 mmol) in acetone (1 mL). After stirring overnight at room temperature, a clear orange solution was obtained. The clear solution was collected and poured into 10 mL diethyl ether. The precipitate thus obtained was filtered off, washed by 1 mL diethyl ether for three times, and dried over vacuum to give the product as an orange powder (yield > 90%). ^{1}H NMR (400 MHz, DMSO-d_6, ppm): δ 10.52 (s, 1H, NHd), 9.42 (s, 1H, NHc), 9.41 (s, 1H, NHb), 9.24 (1, 1H, Ha), 7.96 (d, 2H, *J* = *8.0 Hz*, H3), 7.87 (m, 2H, H1/6), 7.78 (m, 4H, H8/9), 7.71 (d, 2H, *J* = *8.0 Hz*, H7), 7.51-7.41 (m, 3H, H10/11), 7.04-7.00 (m, 3H, H2/4/5).

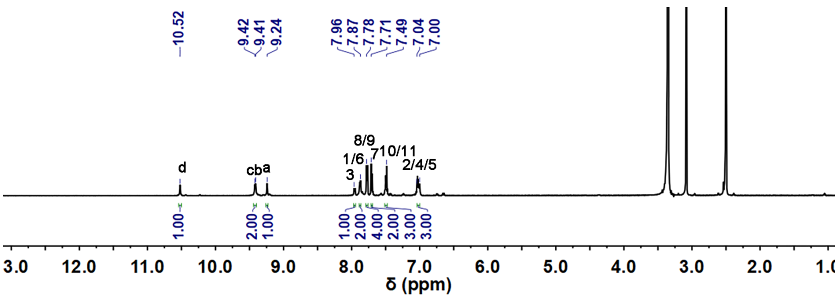

Fig S9. ^{1}H NMR spectrum of complex $(TMA)_2[(SO_4)]_1(\mathbf{L^1})_1$ (***EE*-5**) (400 MHz, DMSO-d_6, 298 K).

$(TMA)_2[(Cl)]_2(L^1)_1$ (complex *EE*-6)

TMACl (48 µL, 0.625 mol/L) was added to a suspension of **L**[1] (10 mg, 6 mmol) in acetone (1 mL). After stirring overnight at room temperature, a clear orange solution was obtained. The clear solution was collected and poured into 10 mL diethyl ether. The precipitate thus obtained was filtered off, washed by 1 mL diethyl ether for three times, and dried over vacuum to give the product as an orange powder (yield > 90%). ^{1}H NMR (400 MHz, DMSO-d_6, ppm): δ 9.83 (s, 1H, NHd), 8.67 (s, 1H, NHc), 8.58 (s, 1H, NHb), 8.47 (s, 1H, Ha), 7.82-7.78 (m, 5H, H6/7/9), 7.65 (m, 3H, H3/8), 7.55-7.51 (m, 4H, H2/8/11), 7.11-7.06 (m, 2H, H4/5).

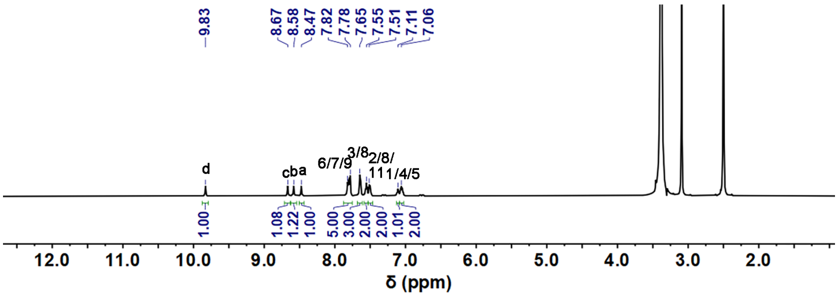

Fig S10. ^{1}H NMR spectrum of complex $(TMA)_2[(Cl)]_2(\mathbf{L^1})_1$ (***EE*-6**) (400 MHz, DMSO-d_6, 298 K).

$(TEA)_2[(Br)]_2(L^1)_1$ (complex *EE*-7)

TEACl (48 μL, 0.625 mol/L) was added to a suspension of $\mathbf{L^1}$ (10 mg, 6 mmol) in acetone and chloroform (1 mL). After stirring overnight at room temperature, a clear orange solution was obtained. Slow vapor diffusion of diethyl ether into this solution provided orange crystals of $(TEA)_2[(Br)]_2(\mathbf{L^1})_1$ with two weeks (yield > 90%). ^{1}H NMR (400 MHz, DMSO-d_6, ppm): δ 9.59 (s, 1H, NHd), 8.54 (s, 1H, NHc), 8.50 (s, 1H, NHb), 8.24 (s, 1H, Ha), 7.84-7.66 (m, 4H, H3/6/7), 7.51-7.11 (m, 8H, H9/2/8/10/11), 7.11-7.06 (m, 3H, H1/4/5).

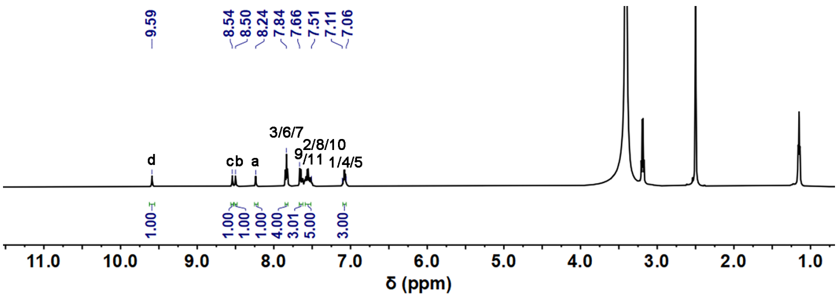

Fig S11. ^{1}H NMR spectrum of complex $(TEA)_2[(Br)]_2(\mathbf{L^1})_1$ (***EE*-7**) (400 MHz, DMSO-d_6, 298 K).

S4. NMR spectroscope

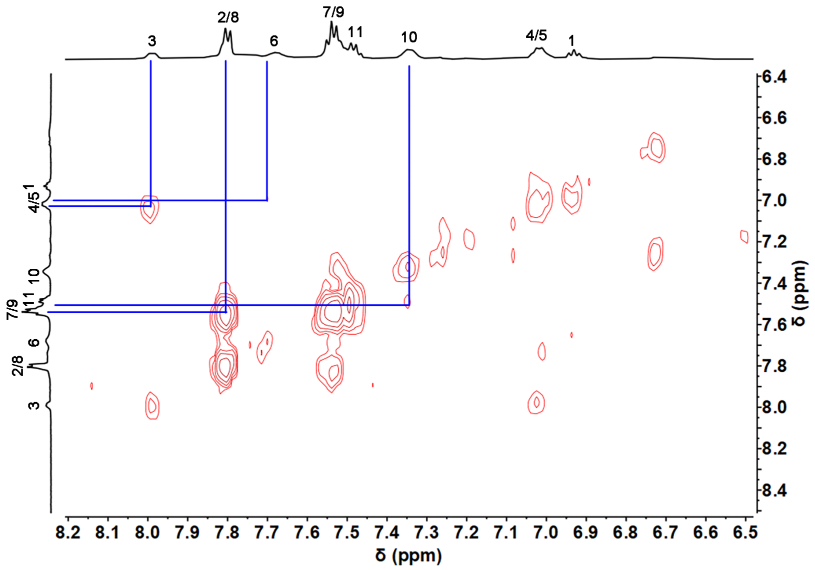

Fig S12. Partial ^{1}H-^{1}H COSY spectrum of ***EE*-3** (600 MHz, DMSO-d_6, 298 K).

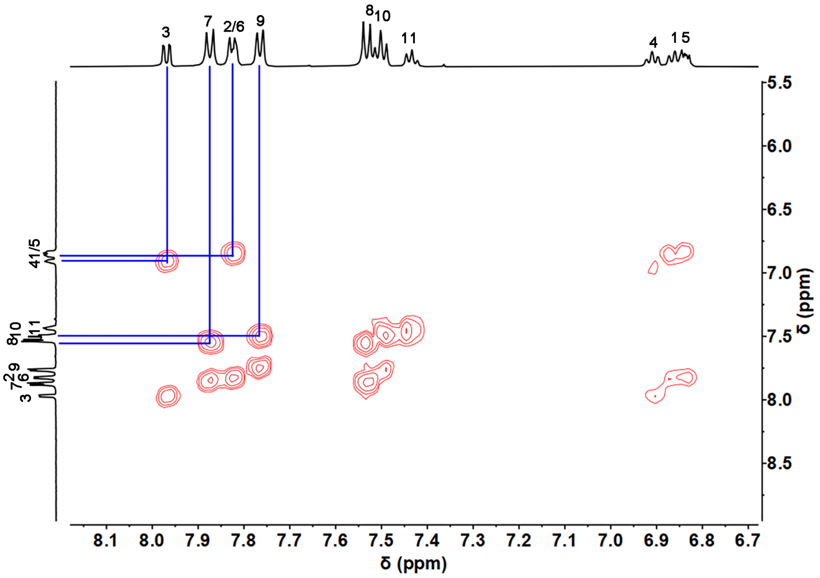

Fig S13. Partial ^{1}H-^{1}H COSY spectrum of ***EE*-4** (600 MHz, DMSO-d_6, 298 K).

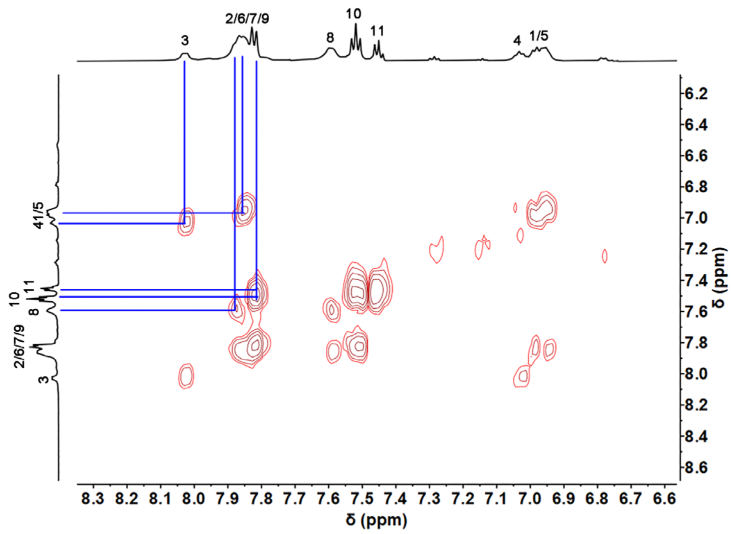

Fig S14. Partial ^{1}H-^{1}H COSY spectrum of ***EE*-4** (600 MHz, CD_3CN, 298 K).

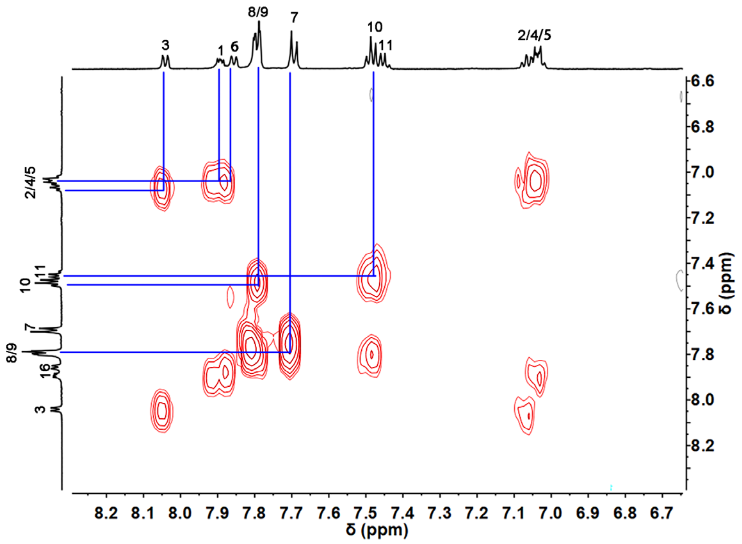

Fig S15. Partial ^{1}H-^{1}H COSY spectrum of ***EE*-5** (600 MHz, CD_3CN, 298 K).

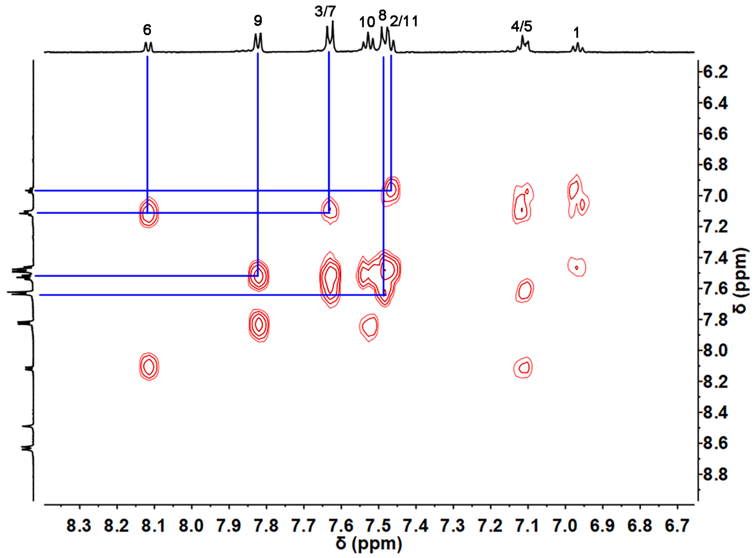

Fig S16. Partial ^{1}H-^{1}H COSY spectrum of ***EE*-6** (600 MHz, CD_3CN, 298 K).

S5. Job's plot Studies

All UV-Vis titrations were performed at room temperature. Certain equivalents of a concentrated anion solution were added stepwise to a 3 mL solution of $\mathbf{L^1}$ in DMSO. As a very small volume of guest solution was added, the final amount of the solution was almost unchanged (3 mL). Solutions of the host $\mathbf{L^1}$ and anion at the same concentration (10 μM) were prepared in DMSO, used for determining the binding stoichiometry. Then the two solutions were mixed in different proportions maintaining a total volume of 3 mL and a total concentration of 10 μM. After incubating the mixture for 30 s, the spectra of the solutions for different compositions were recorded. The data was then collated and combined to produce data files from which so-called Job plots could be constructed.

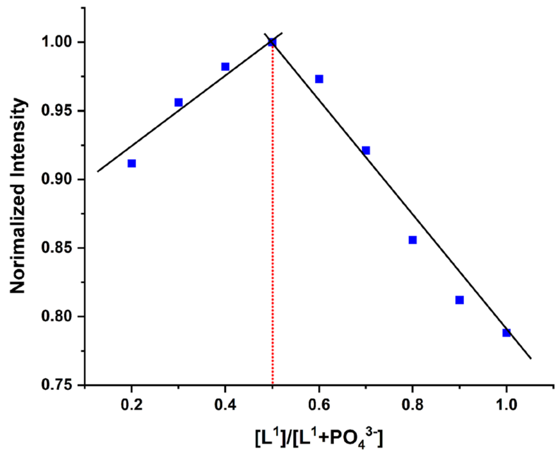

Fig S17. $\mathbf{L^1}$ (10 μM) with PO_4^{3-} Job's plot.

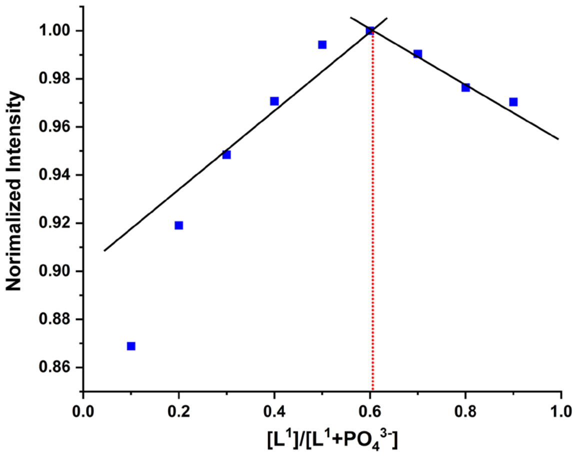

Fig S18. L^1 (10 μM) with PO_4^{3-} Job's plot.

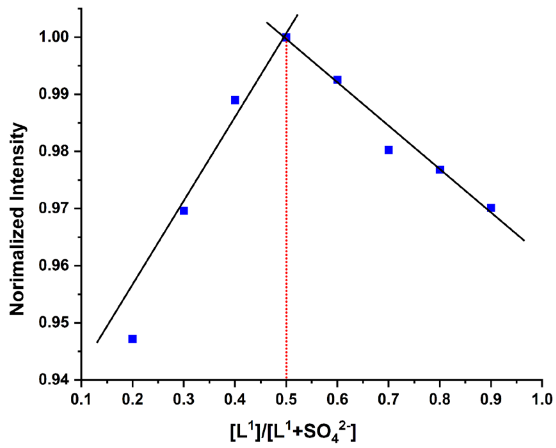

Fig S19. L^1 (10 μM) with SO_4^{2-} Job's plot.

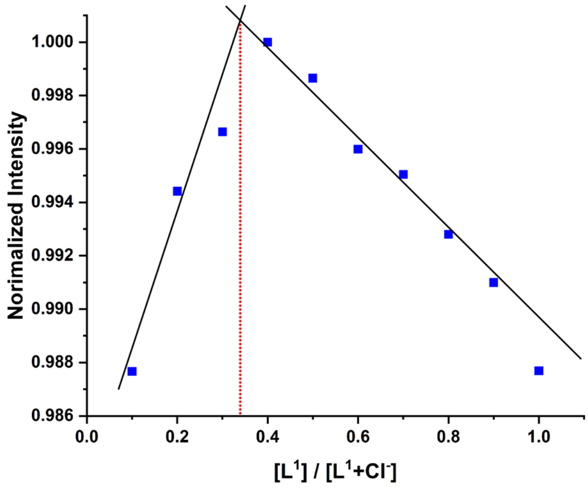

Fig S20. L^1 (10 μM) with Cl^- Job's plot.

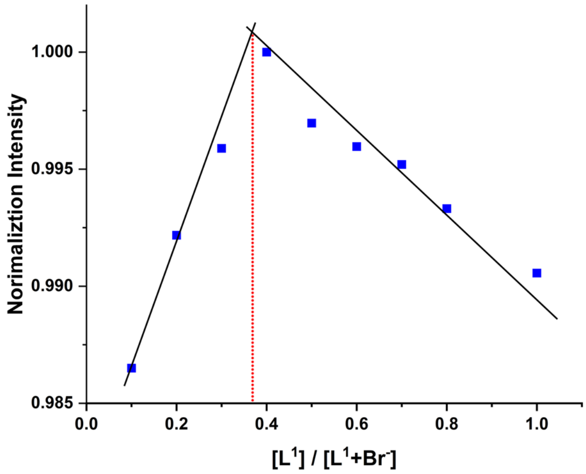

Fig S21. L[1] (10 μM) with Br⁻ Job's plot.

S6. Photoisomerization Studies

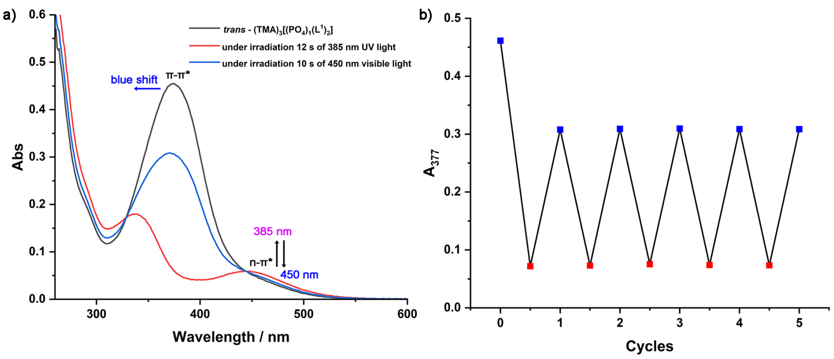

Fig S22. a) UV−vis absorption spectra of **$(TMA)_3[(PO_4)_1(L^1)_2]$** under altering light irradiation (385 nm and 450 nm, 3W) and b) changes of absorbance intensity at 377 nm. (5 μM in DMSO).

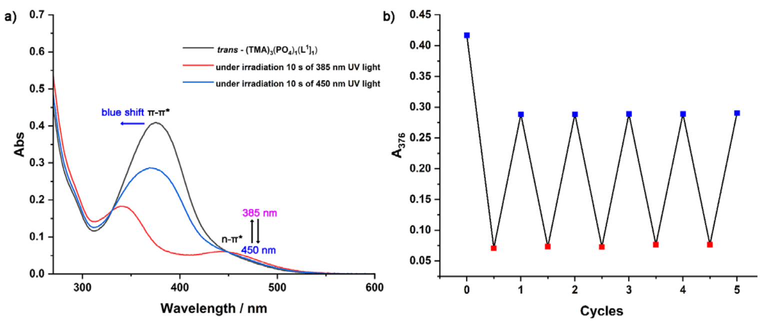

Fig S23. a) UV−vis absorption spectra of **$(TMA)_3[(PO_4)_1(L^1)_1]$** under altering light irradiation (385 nm and 450 nm, 3W) and b) changes of absorbance intensity at 376 nm. (10 μM in DMSO).

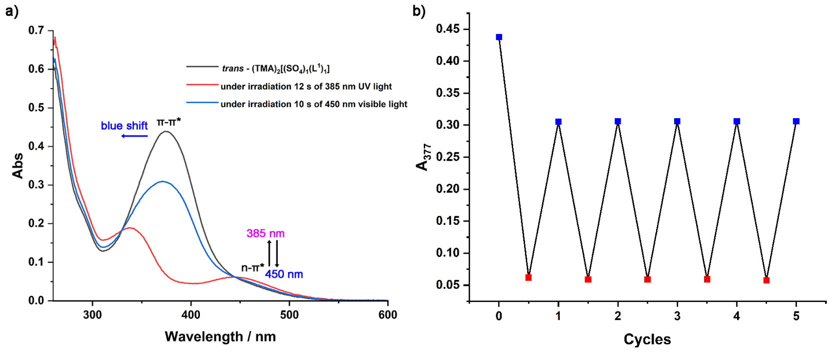

Fig S24. a) UV−vis absorption spectra of **$(TMA)_2[(SO_4)_1(L^1)_1]$** under altering light irradiation (385 nm and 450 nm, 3W) and b) changes of absorbance intensity at 377 nm. (10 μM in DMSO).

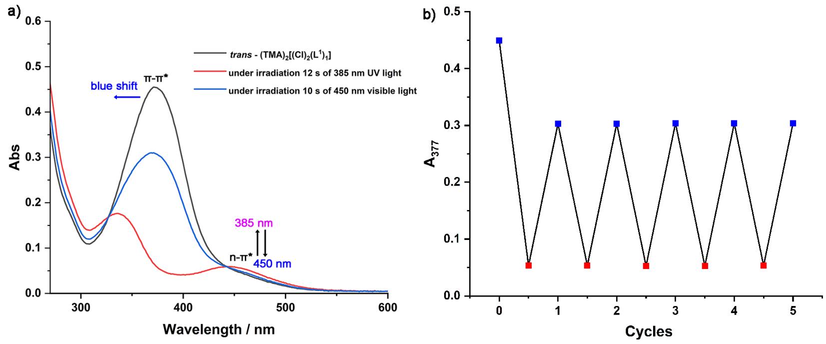

Fig S25. a) UV−vis absorption spectra of **$(TMA)_2[(Cl)_2(L^1)_1]$** under altering light irradiation (385 nm and 450 nm, 3W) and b) changes of absorbance intensity at 377 nm. (10 μM in DMSO).

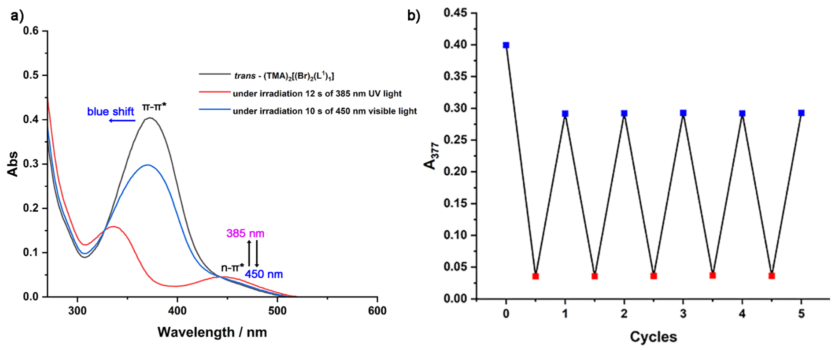

Fig S26. a) UV−vis absorption spectra of **$(TMA)_2[(Br)_2(L^1)_1]$** under altering light irradiation (385 nm and 450 nm, 3W) and b) changes of absorbance intensity at 377 nm. (10 μM in DMSO).

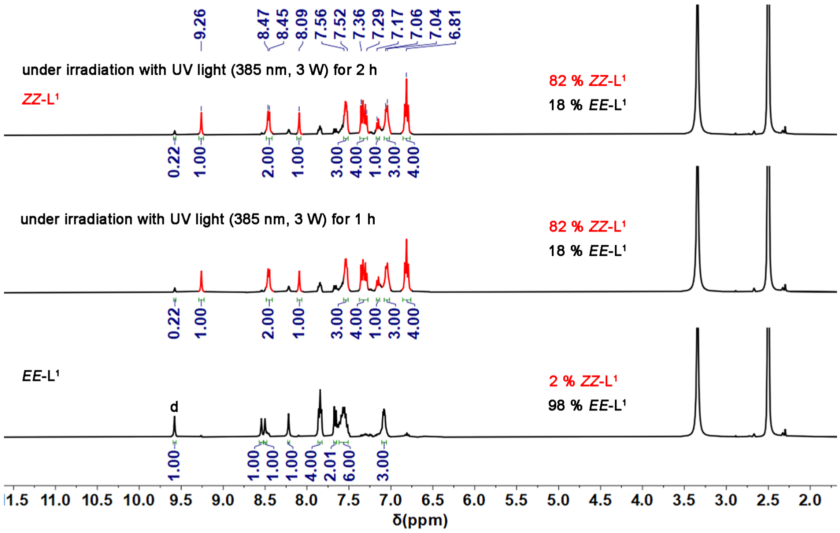

Fig S27. ^{1}H NMR spectra of ***EE*-L^{1}** under irradiation with UV light (385 nm 3W) for different time (400 MHz, DMSO-d_6, 298 K) (***EE*-L^{1}**, labeled in black; ***ZZ* -L^{1}**, labeled in red).

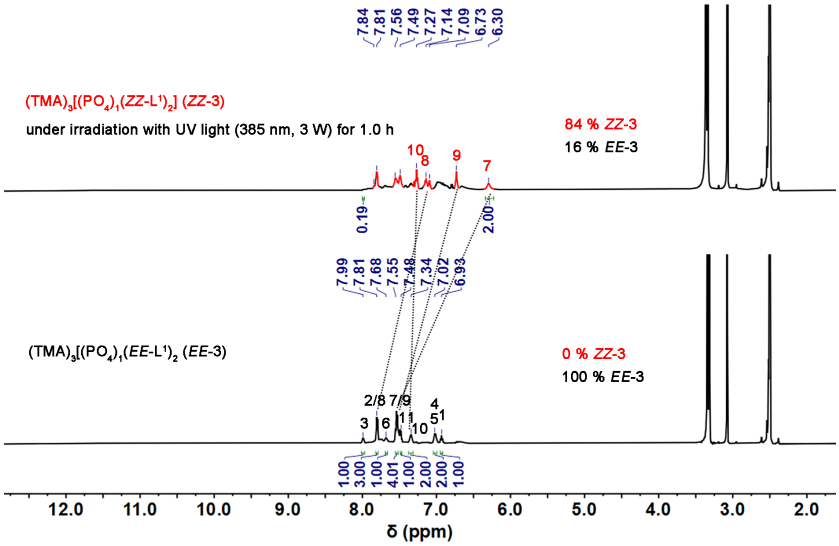

Fig S28. ^{1}H NMR spectra of ***EE*-3** under irradiation with UV light (385 nm 3 W) for 1.0 h (400 MHz, DMSO-d_6, 298 K) (***EE*-3**, labeled in black; ***ZZ*-3**, labeled in red).

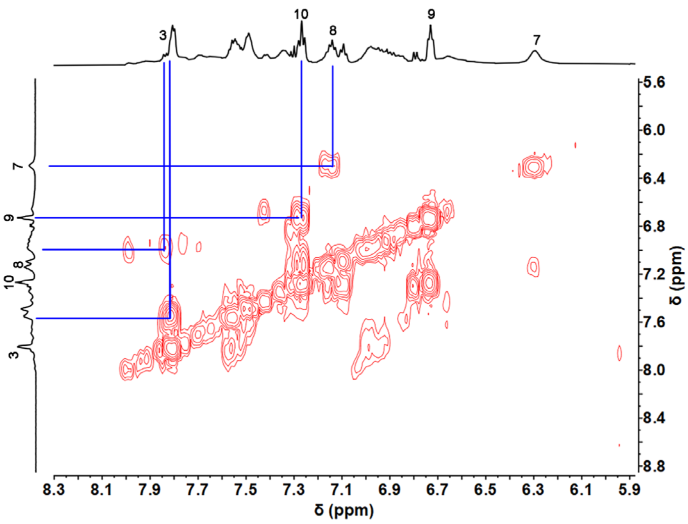

Fig S29. Partial ^{1}H-^{1}H COSY spectrum of ***ZZ*-3** (400 MHz, DMSO-d_6, 298 K).

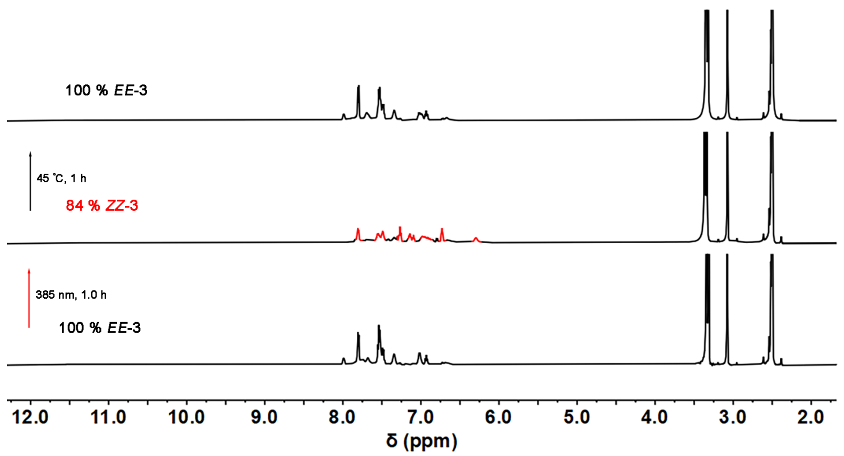

Fig S30. ^{1}H NMR spectra of ***EE*-3** upon heating at 45 °C for 1 h (400 MHz, DMSO-d_6, 298 K) (***EE*-3**, labeled in black; ***ZZ*-3**, labeled in red).

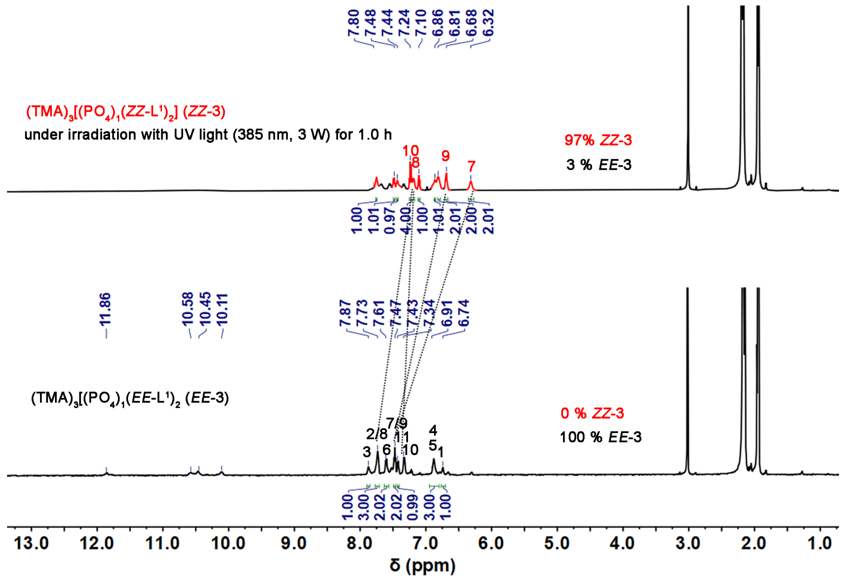

Fig S31. ^{1}H NMR spectra of ***EE*-3** under irradiation with UV light (385 nm 3 W) for 1.0 h (400 MHz, CD_3CN, 298 K) (***EE*-3**, labeled in black; ***ZZ*-3**, labeled in red).

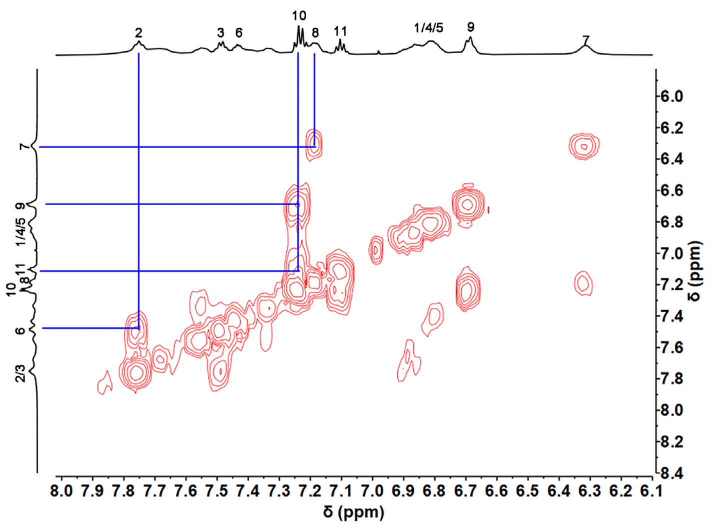

Fig S32. Partial ^{1}H-^{1}H COSY spectrum of ***ZZ*-3** (400 MHz, CD_3CN, 298 K).

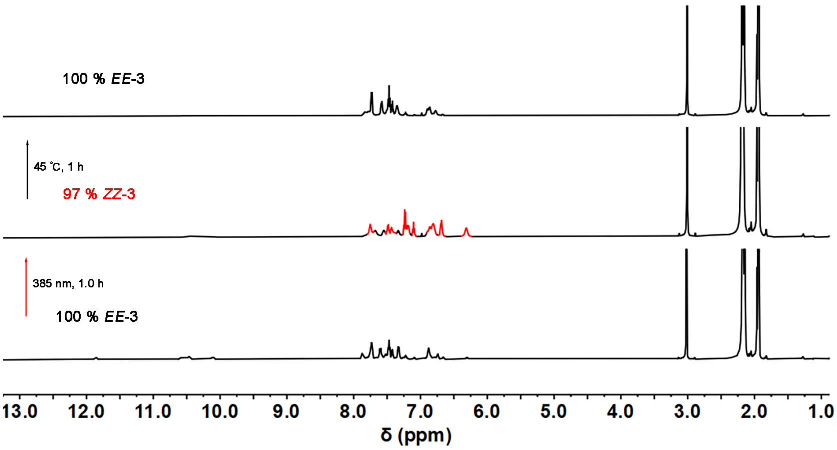

Fig S33. [1]H NMR spectra of ***ZZ*-3** upon heating at 45 °C for 1 h (400 MHz, CD_3CN, 298 K) (***EE*-3**, labeled in black; ***ZZ*-3**, labeled in red).

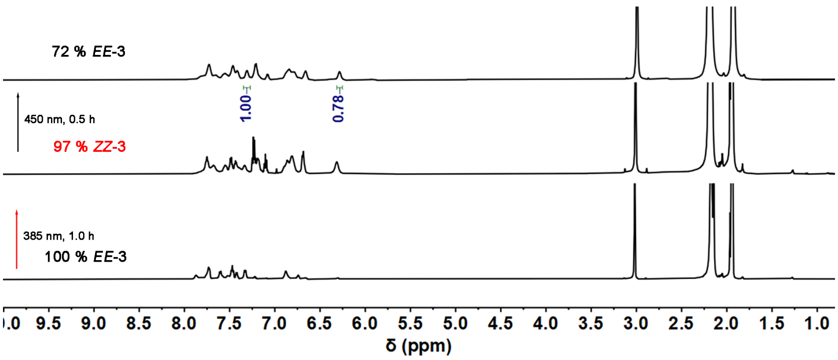

Fig S34. [1]H NMR spectra of ***ZZ*-3** irradiation with visible light (450 nm 3 W) for 0.5 h (400 MHz, CD_3CN, 298 K).

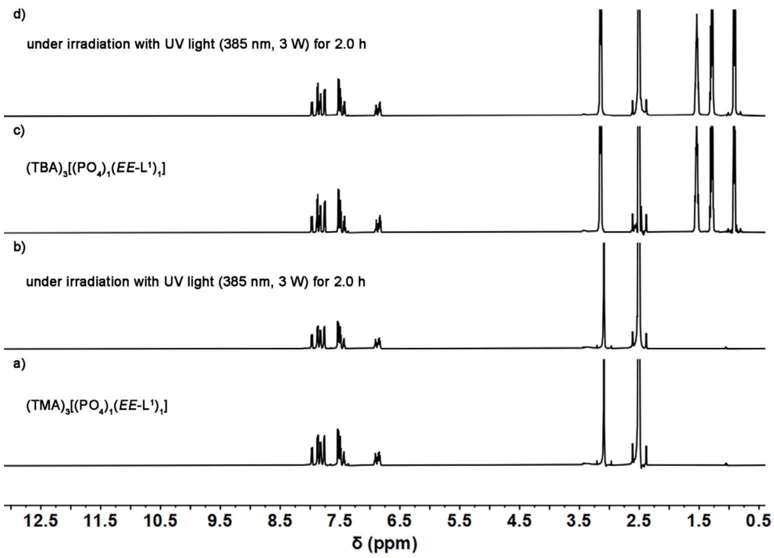

Fig S35. [1]H NMR spectra of a) $(TMA)_3[(PO_4)_1($***EE*-L**$^1)_1]$ and c) $(TBA)_3[(PO_4)_1($***EE*-L**$^1)_1]$ (**L**^{1} = 2 mM) under irradiation with UV light (385 nm 3 W) for 2.0 h (400 MHz, DMSO-d_6, 298 K).

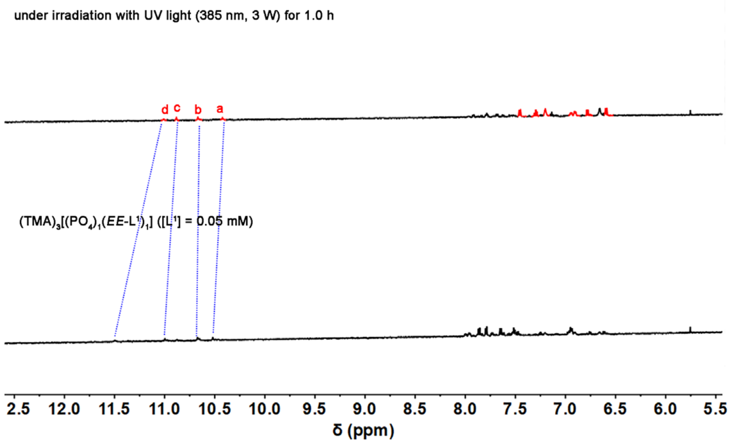

Fig S36. Partial ^{1}H NMR spectra of $(TMA)_3[(PO_4)_1(\textbf{\textit{EE}}\text{-}\mathbf{L^1})_1]$ ($\mathbf{L^1}$ = 0.05 mM) under irradiation with UV light (385 nm 3 W) for 1.0 h (400 MHz, DMSO-d_6, 298 K).

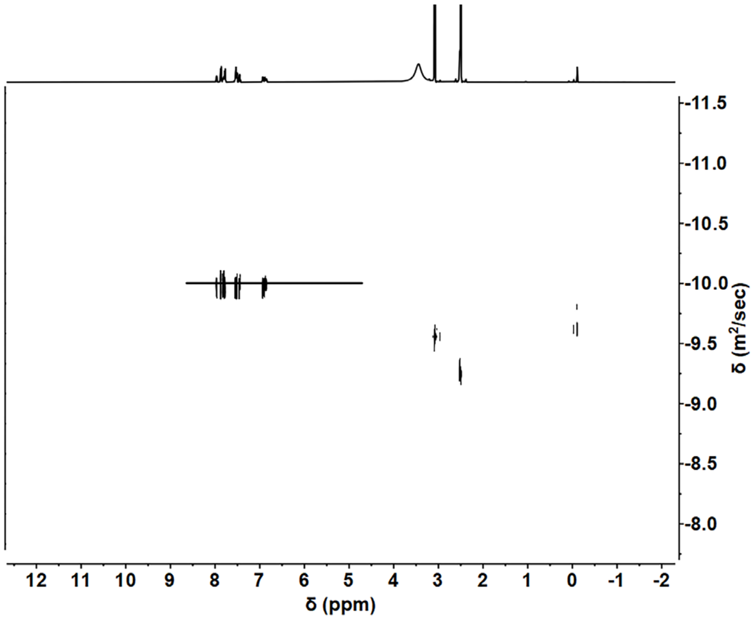

Fig S37. DOSY spectrum of $(TMA)_3[(PO_4)_1(\textbf{\textit{EE}}\text{-}\mathbf{L^1})_1]$ ($\mathbf{L^1}$ = 2 mM) (400 MHz, DMSO-d_6, 298 K).

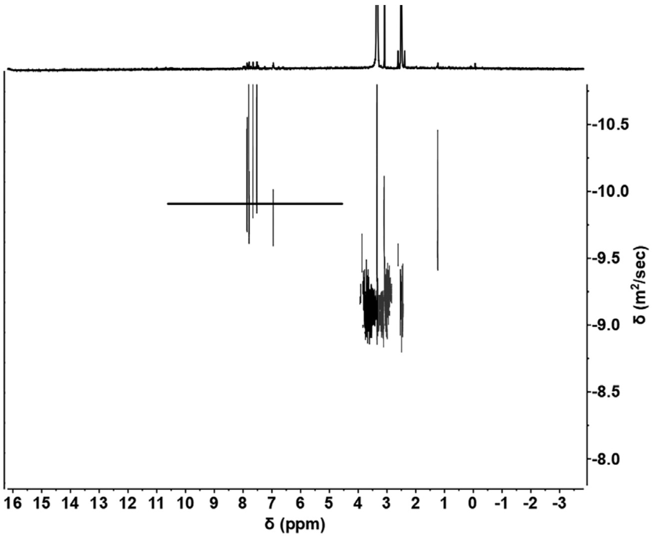

Fig S38. DOSY spectrum of $(TMA)_3[(PO_4)_1(\textbf{\textit{EE}}\text{-}\mathbf{L^1})_1]$ ($\mathbf{L^1}$ = 0.05 mM) (400 MHz, DMSO-d_6, 298 K).

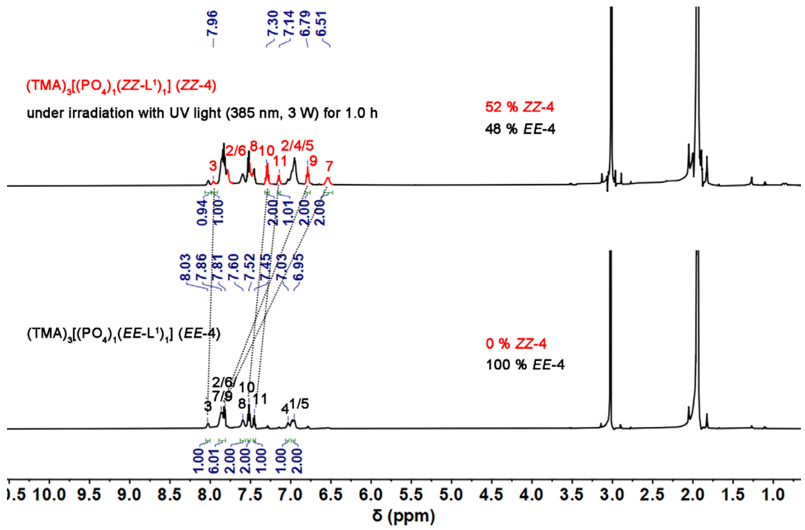

Fig S39. [1]H NMR spectra of $(TMA)_3[(PO_4)_1(\boldsymbol{EE}\text{-}\mathbf{L^1})_1]$ ($\mathbf{L^1}$ = 2 mM) under irradiation with UV light (385 nm 3 W) for 1.0 h (400 MHz, CD_3CN, 298 K).

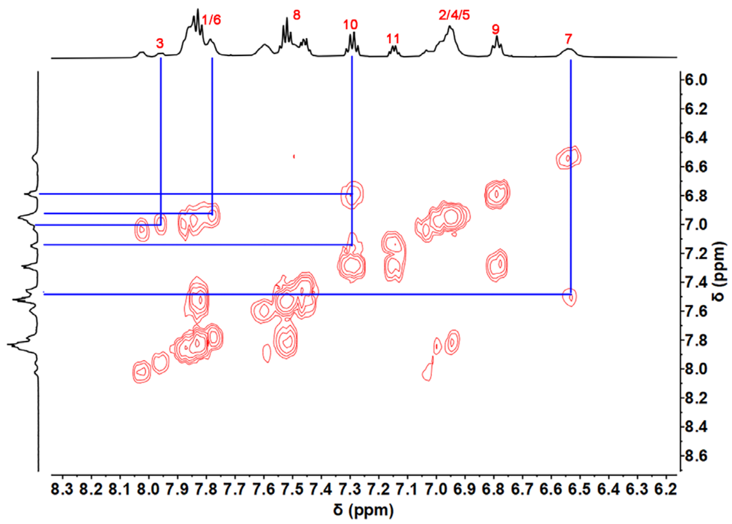

Fig S40. Partial [1]H-[1]H COSY spectrum of ***ZZ*-4** (400 MHz, CD_3CN, 298 K).

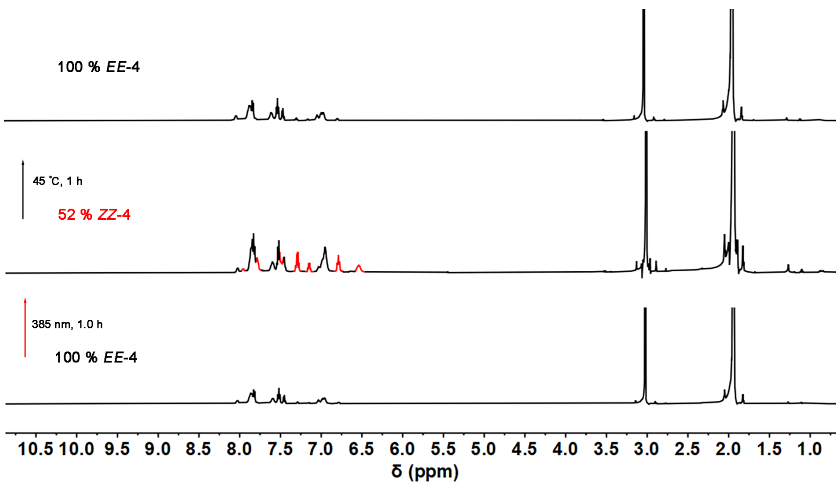

Fig S41. [1]H NMR spectra of ***ZZ*-4** upon heating at 45 °C for 1 h (400 MHz, CD_3CN, 298 K) (***EE*-4**, labeled in black; ***ZZ*-4**, labeled in red).

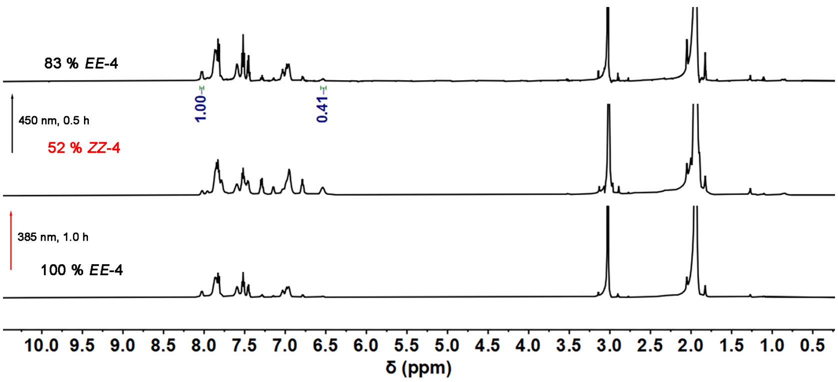

Fig S42. ^{1}H NMR spectra of ***ZZ-4*** irradiation with visible light (450 nm 3 W) for 0.5 h (400 MHz, CD_3CN, 298 K).

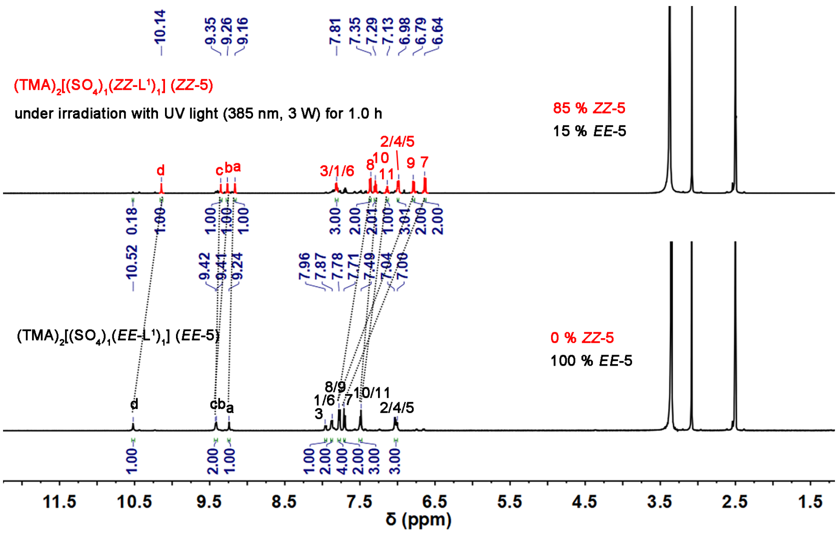

Fig S43. ^{1}H NMR spectra of ***EE*-5** under irradiation with UV light (385 nm 3 W) for 0.5 h (400 MHz, DMSO-d_6, 298 K) (***EE*-5**, labeled in black; ***ZZ*-5**, labeled in red).

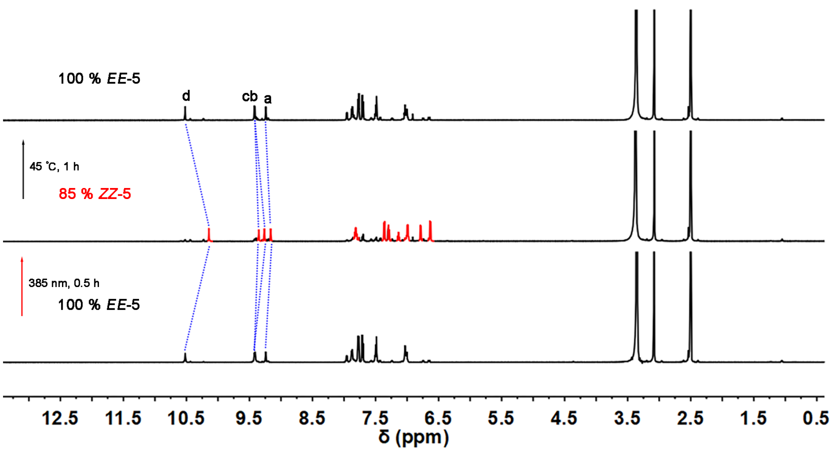

Fig S44. ^{1}H NMR spectra of ***ZZ*-5** upon heating at 45 °C for 1 h (400 MHz, DMSO-d_6, 298 K) (***EE*-5**, labeled in black; ***ZZ*-5**, labeled in red).

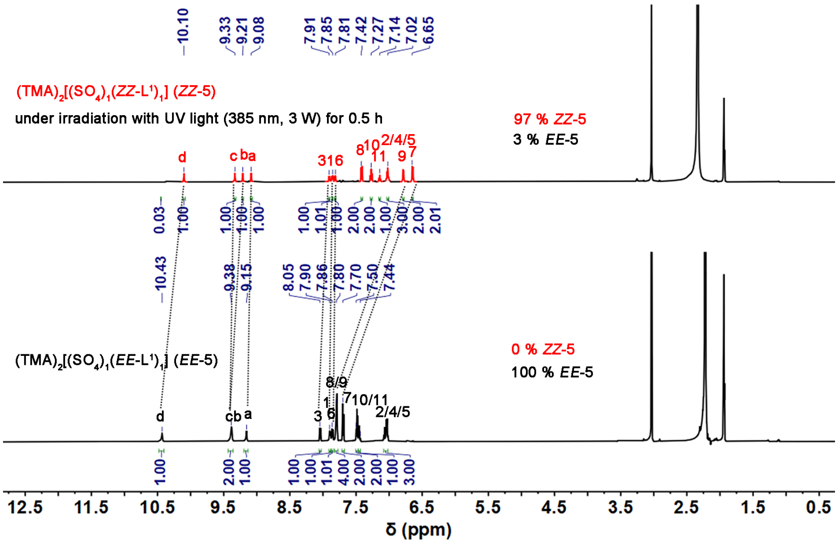

Fig S45. [1]H NMR spectra of ***EE*-5** under irradiation with UV light (385 nm 3 W) for 0.5 h (400 MHz, CD_3CN, 298 K) (***EE*-5**, labeled in black; ***ZZ*-4**, labeled in red).

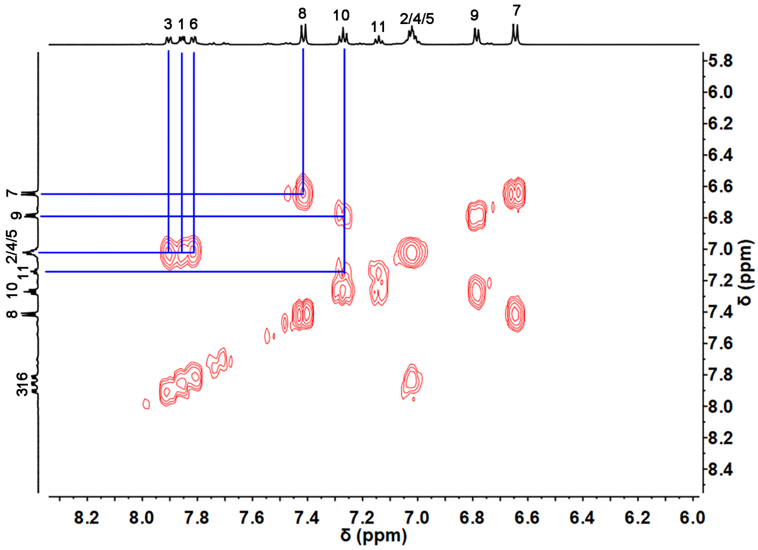

Fig S46. Partial [1]H-[1]H COSY spectrum of ***ZZ*-5** (400 MHz, CD_3CN, 298 K).

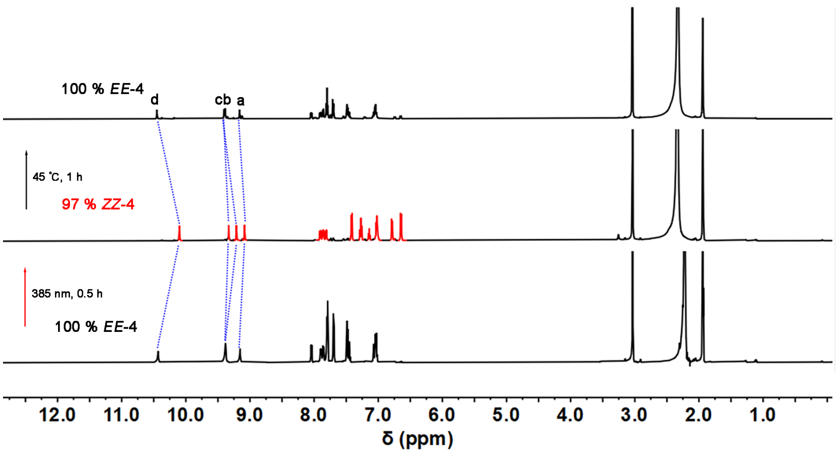

Fig S47. [1]H NMR spectra of ***ZZ*-5** upon heating at 45 °C for 1 h (400 MHz, CD_3CN, 298 K) (***EE*-5**, labeled in black; ***ZZ*-5**, labeled in red).

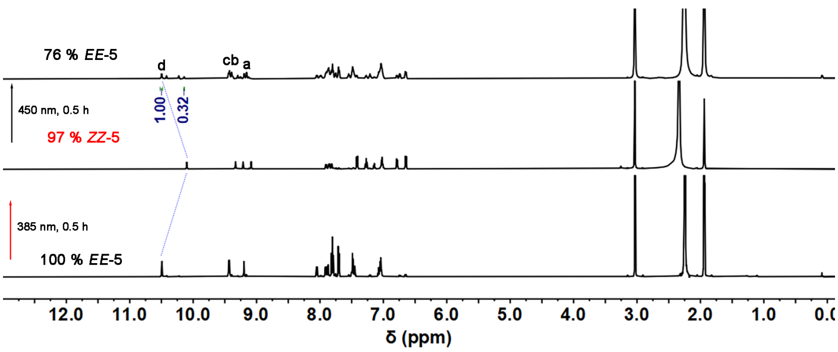

Fig S48. [1]H NMR spectra of ***ZZ*-5** irradiation with visible light (450 nm 3 W) for 0.5 h (400 MHz, CD_3CN, 298 K).

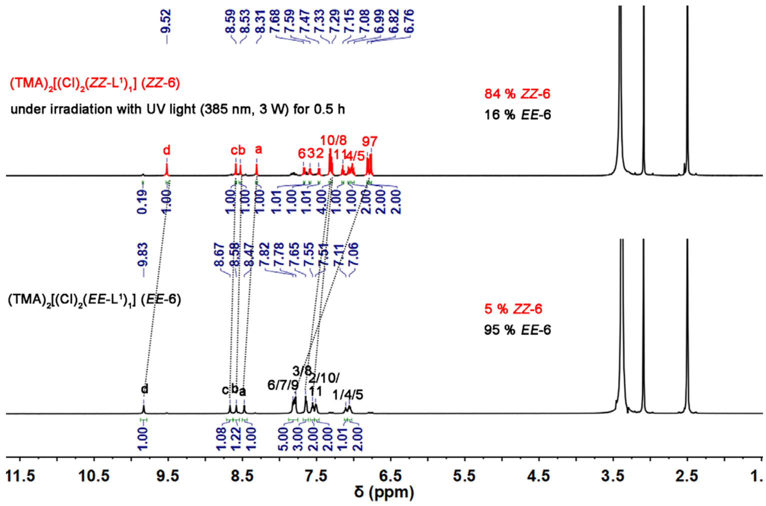

Fig S49. [1]H NMR spectra of ***EE*-6** under irradiation with UV light (385 nm 3 W) for 0.5 h (400 MHz, DNSO-d_6, 298 K) (***EE*-6**, labeled in black; ***ZZ*-6**, labeled in red).

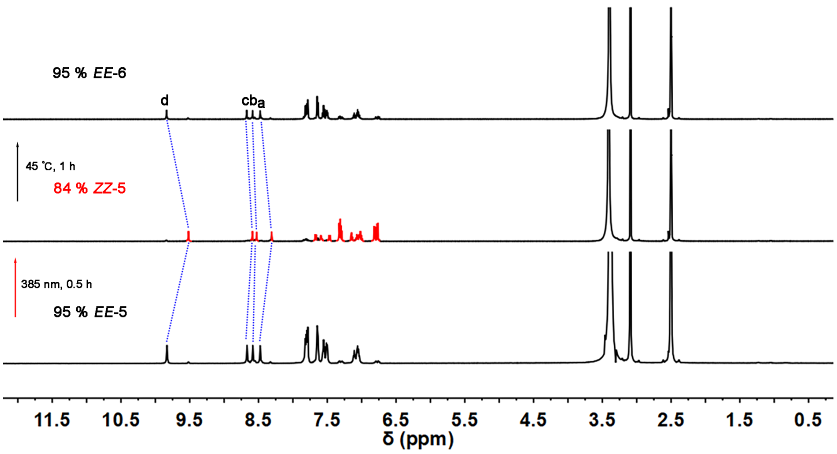

Fig S50. [1]H NMR spectra of ***ZZ*-6** upon heating at 45 °C for 1 h (400 MHz, DNSO-d_6, 298 K) (***EE*-6**, labeled in black; ***ZZ*-6**, labeled in red).

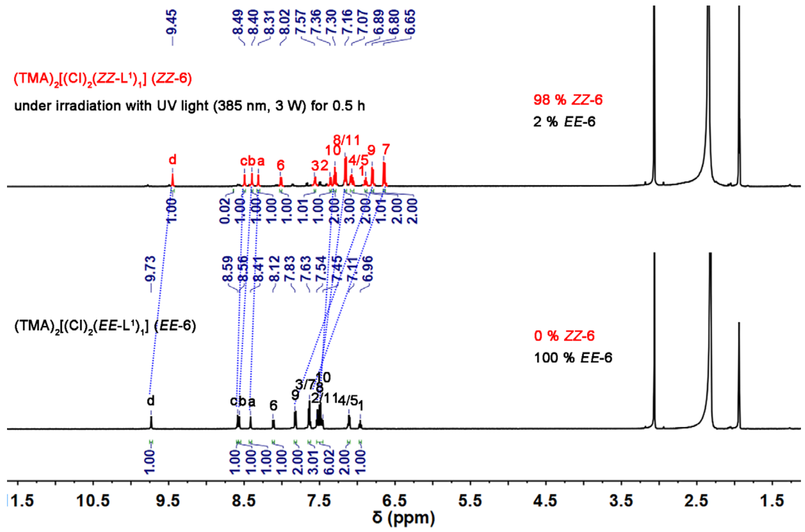

Fig S51. ^{1}H NMR spectra of ***EE*-6** under irradiation with UV light (385 nm 3 W) for 0.5 h (400 MHz, CD_3CN, 298 K) (***EE*-6**, labeled in black; ***ZZ*-6**, labeled in red).

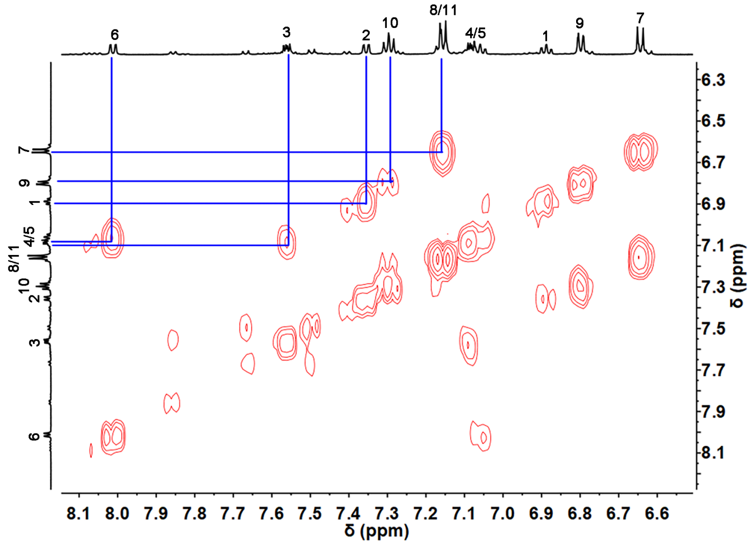

Fig S52. Partial ^{1}H-^{1}H COSY spectrum of ***ZZ*-6** (400 MHz, CD_3CN, 298 K).

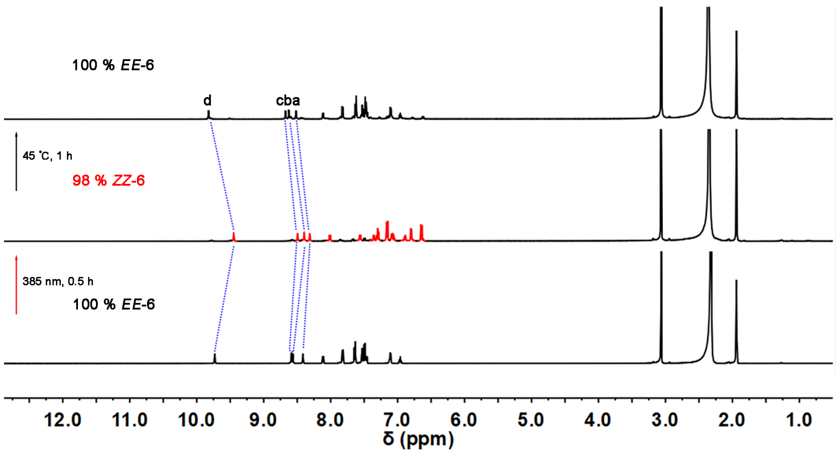

Fig S53. ^{1}H NMR spectra of ***ZZ*-6** upon heating at 45 °C for 1 h (400 MHz, CD_3CN, 298 K) (***EE*-6**, labeled in black; ***ZZ*-6**, labeled in red).

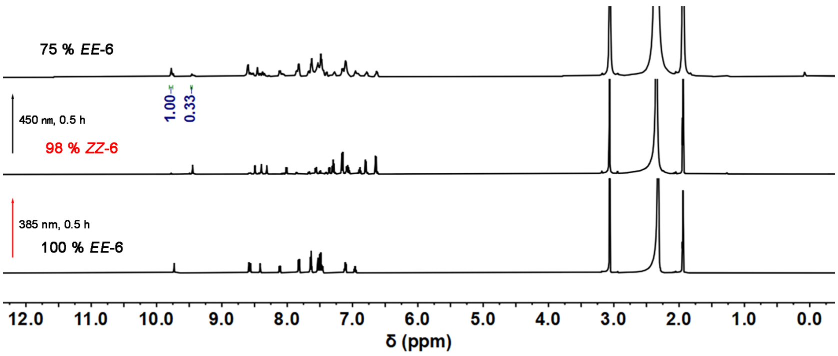

Fig S54. [1]H NMR spectra of ***ZZ-6*** irradiation with visible light (450 nm 3 W) for 0.5 h (400 MHz, CD_3CN, 298 K).

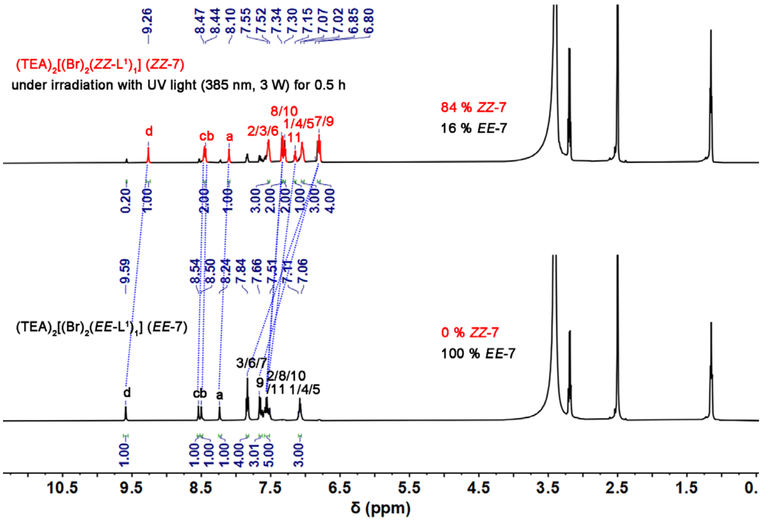

Fig S55. [1]H NMR spectra of ***EE-7*** under irradiation with UV light (385 nm 3 W) for 0.5 h (400 MHz, DNSO-d_6, 298 K) (***EE-7***, labeled in black; ***ZZ-7***, labeled in red).

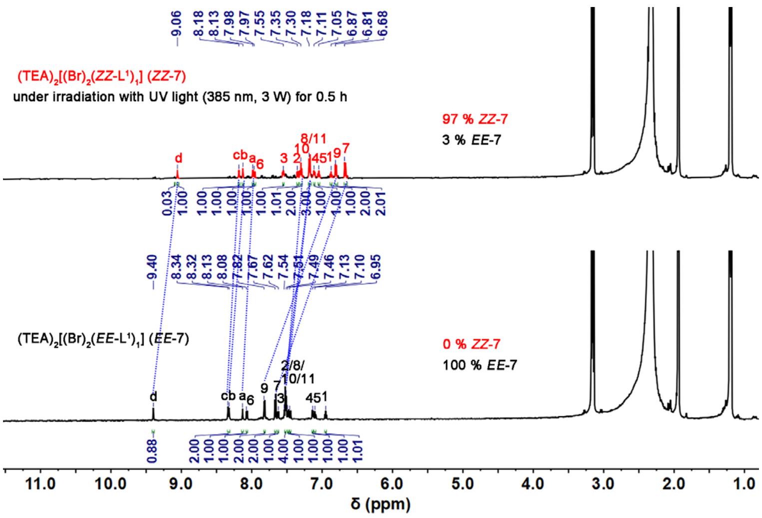

Fig S56. [1]H NMR spectra of ***EE-7*** under irradiation with UV light (385 nm 3 W) for 0.5 h (400 MHz, CD_3CN, 298 K) (***EE-7***, labeled in black; ***ZZ-7***, labeled in red).

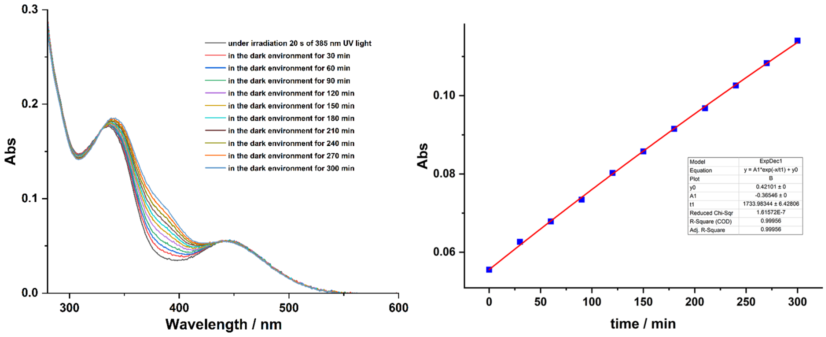

Fig S57. First-order kinetics plot in thermal isomerization of ***ZZ*-L**[1] derived from UV-Vis data.

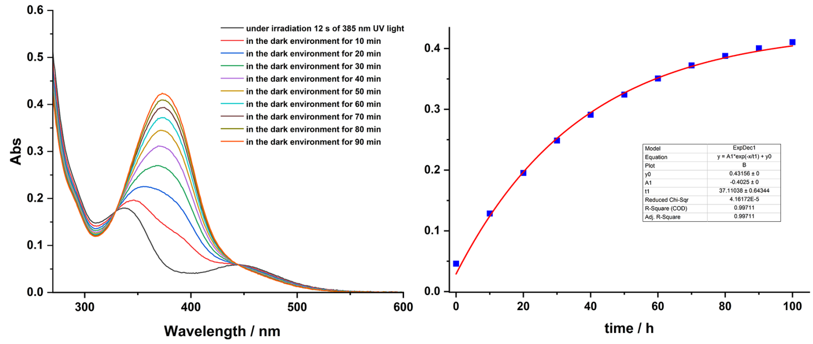

Fig S58. First-order kinetics plot in thermal isomerization of ***ZZ*-3** derived from UV-Vis data.

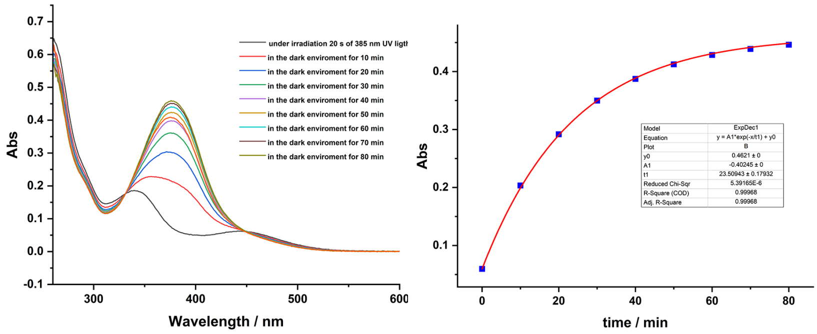

Fig S59. First-order kinetics plot in thermal isomerization of ***ZZ*-4** derived from UV-Vis data.

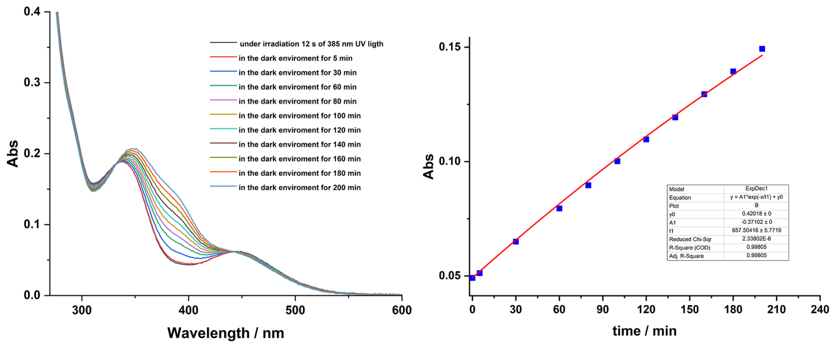

Fig S60. First-order kinetics plot in thermal isomerization of ***ZZ*-5** derived from UV-Vis data.

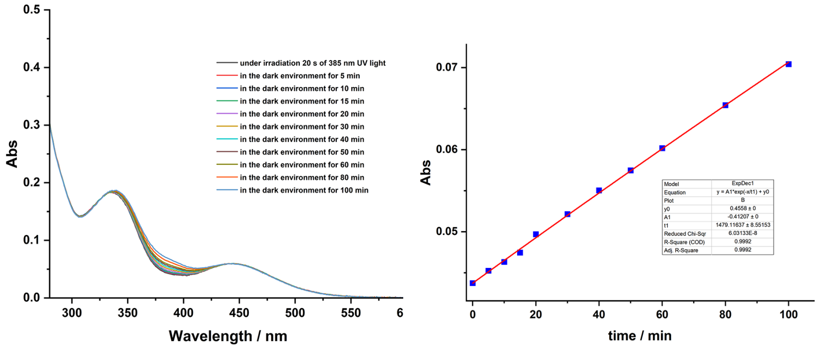

Fig S61. First-order kinetics plot in thermal isomerization of ***ZZ*-6** derived from UV-Vis data.

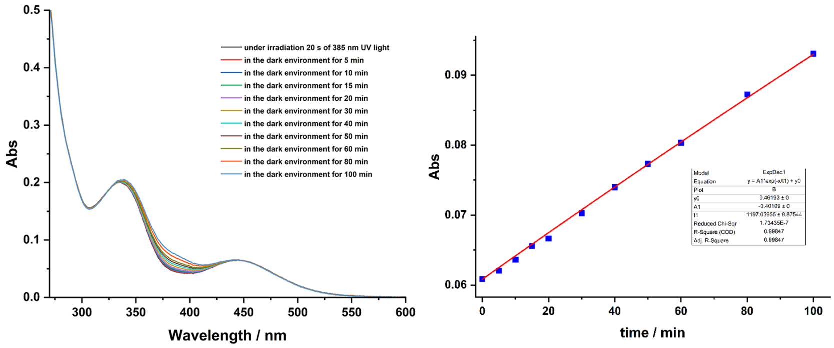

Fig S62. First-order kinetics plot in thermal isomerization of ***ZZ*-7** derived from UV-Vis data.

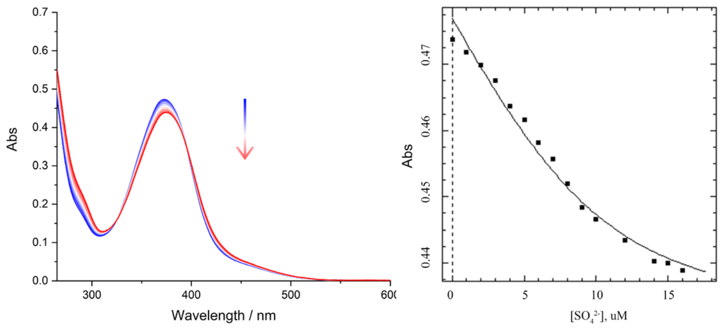

Fig S63. Determination of binding constant of SO_4^{2-} and ***EE*-L[1]** by UV titrations. In UV titrations, successive addition of known amounts of $(TMA)_2SO_4$ was added to a 3.0 mL solution of 0.01 mM ***EE*-L[1]** in DMSO. The association constant was determined by fitting the titration curves to a 1:1 (host : guest) binding mode by the Dynafit program (CV% = 7.8).

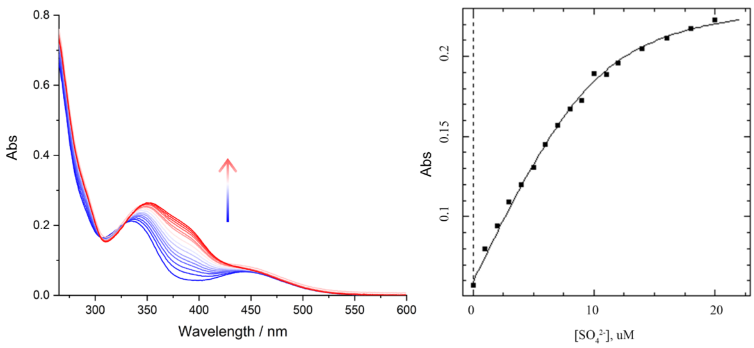

Fig S64. Determination of binding constant of SO_4^{2-} and ***ZZ*-L[1]** by UV titrations. In UV titrations, successive addition of known amounts of $(TMA)_2SO_4$ was added to a 3.0 mL solution of 0.01 mM ***EE*-L**[1] in DMSO. The association constant was determined by fitting the titration curves to a 1:1 (host : guest) binding mode by the Dynafit program (CV% = 4.2).

S7. High-resolution MS studies

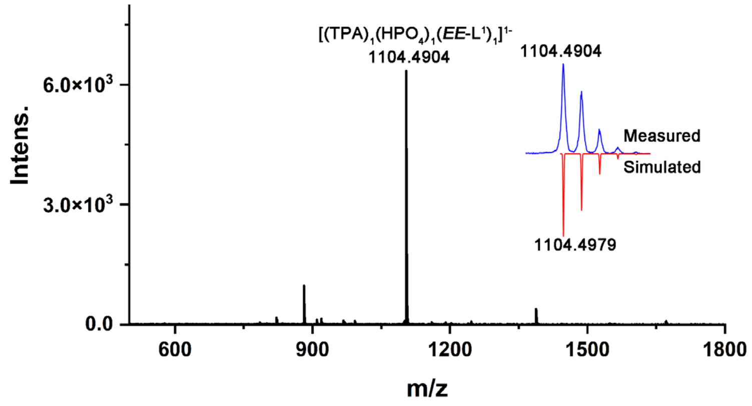

Fig S65. High-resolution ESI-mass spectrum of complex ***EE*-1**.

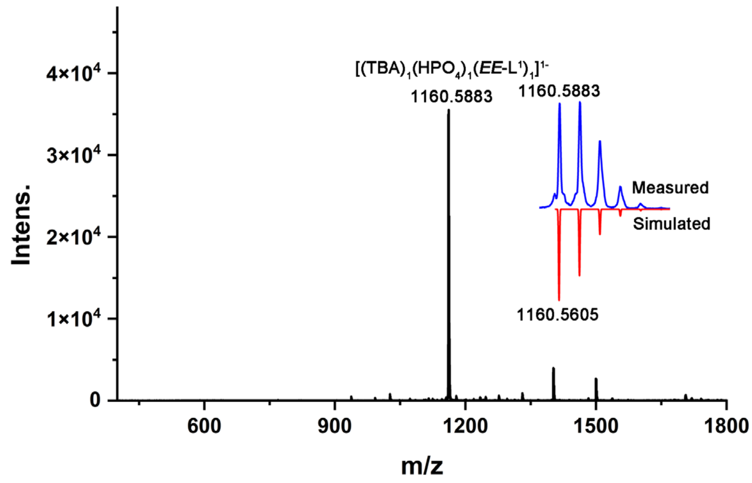

Fig S66. High-resolution ESI-mass spectrum of complex ***EE*-2**.

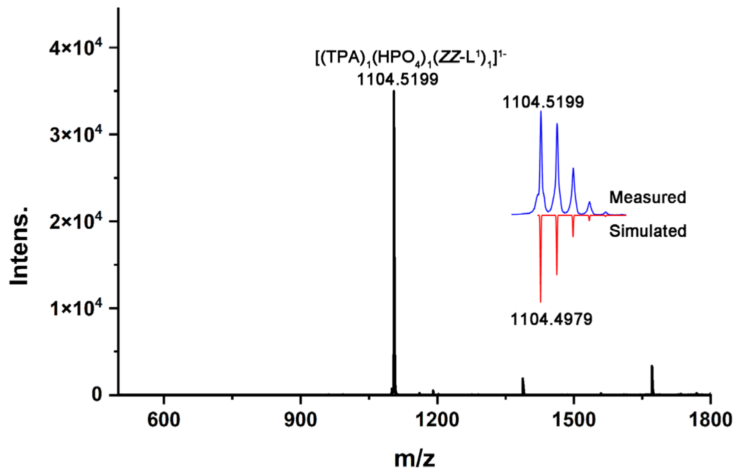

Fig S67. High-resolution ESI-mass spectrum of complex ***ZZ*-1**.

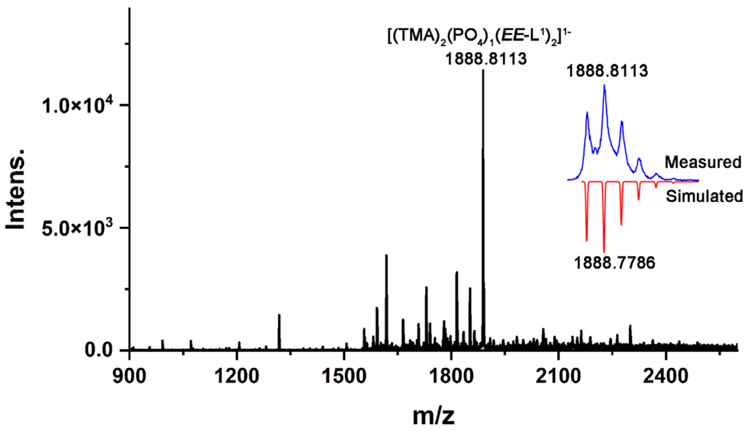

Fig S68. High-resolution ESI-mass spectrum of complex ***EE*-3**.

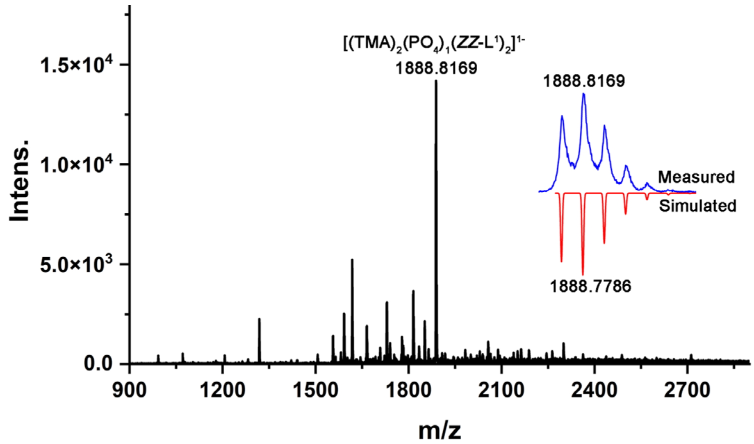

Fig S69. High-resolution ESI-mass spectrum of complex ***ZZ*-3**.

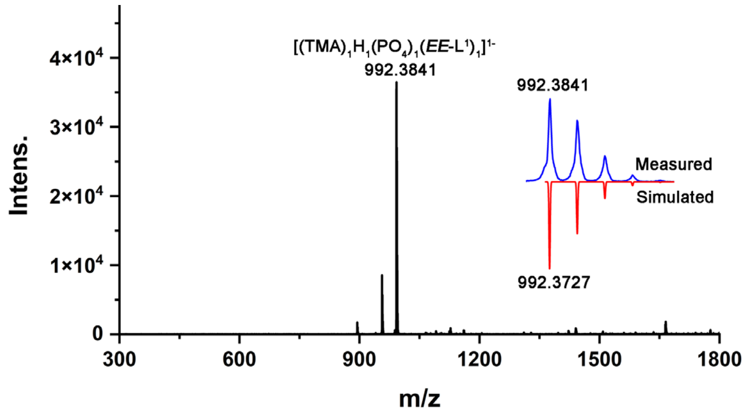

Fig S70. High-resolution ESI-mass spectrum of complex ***EE*-4**.

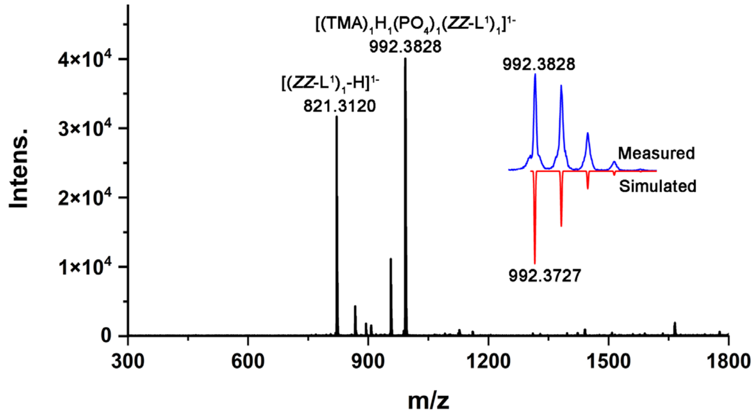

Fig S71. High-resolution ESI-mass spectrum of complex ***ZZ*-4**.

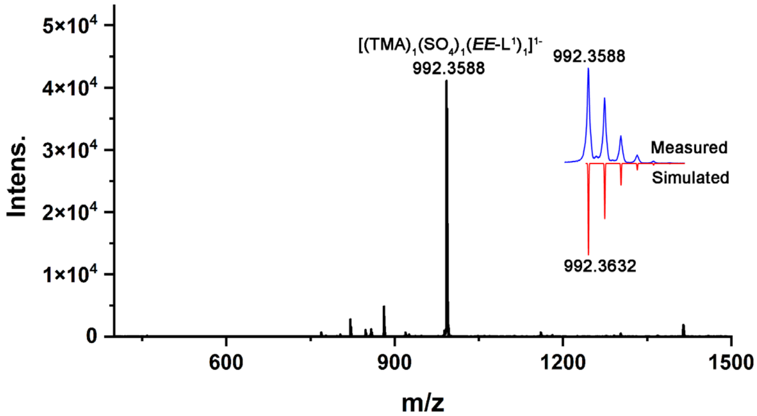

Fig S72. High-resolution ESI-mass spectrum of ***EE*-5**.

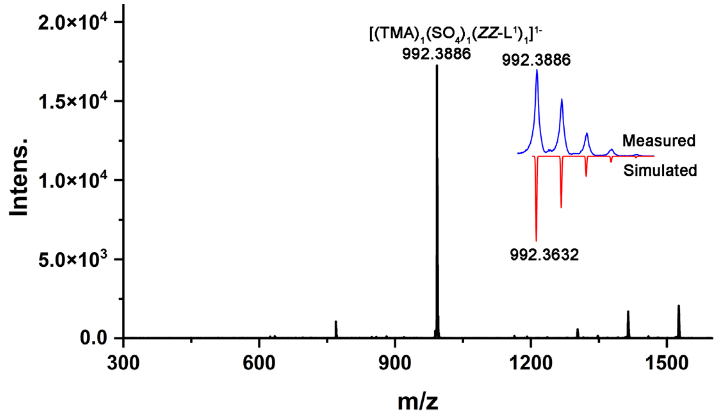

Fig S73. High-resolution ESI-mass spectrum of ***ZZ*-5**.

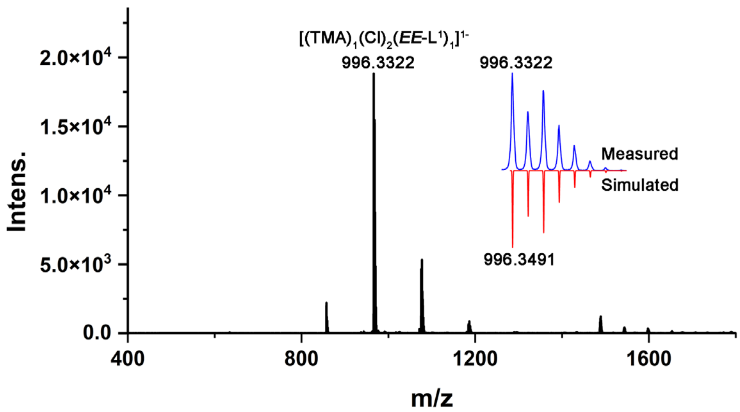

Fig S74. High-resolution ESI-mass spectrum of ***EE*-6**.

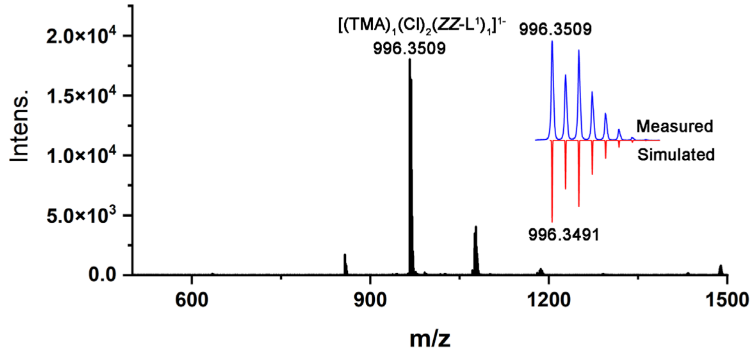

Fig S75. High-resolution ESI-mass spectrum of ***ZZ*-6**.

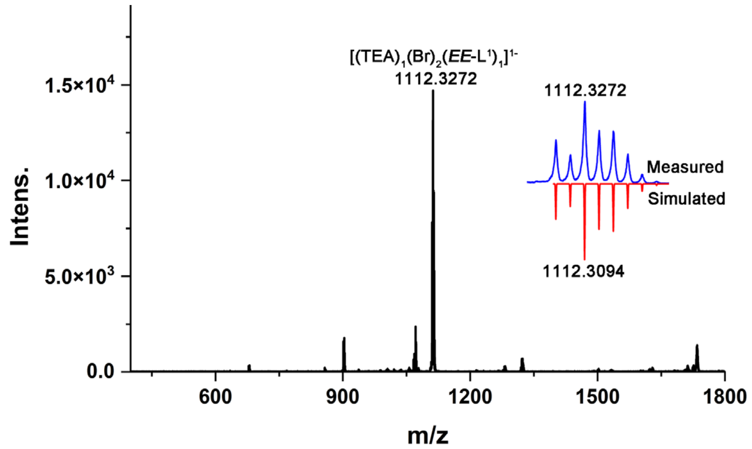

Fig S76. High-resolution ESI-mass spectrum of ***EE*-7**.

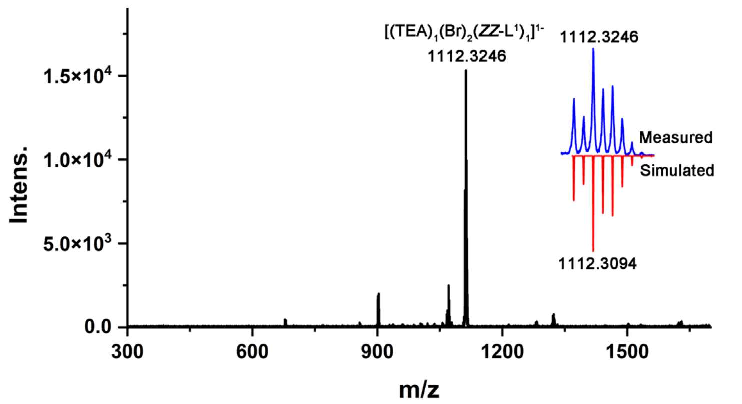

Fig S77. High-resolution ESI-mass spectrum of ***ZZ*-7**.

S8. Crystal Structures of the Guest-Inclusion Complexes

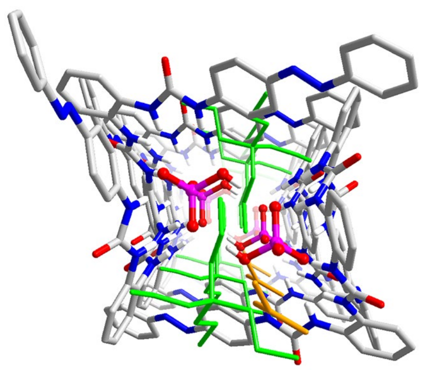

Fig S78. Molecular stacking structure of complex ***EE*-1** along the b-axis in space.

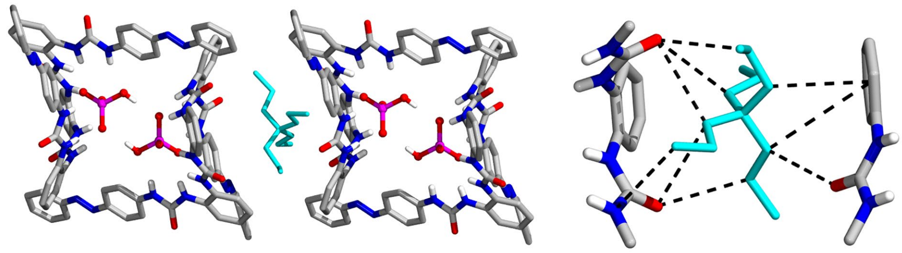

Fig S79. TPA$^+$ cation of outside the pore channel were stabilized through C−H···O, C−H···π, and C−H···N non-covalent interactions.

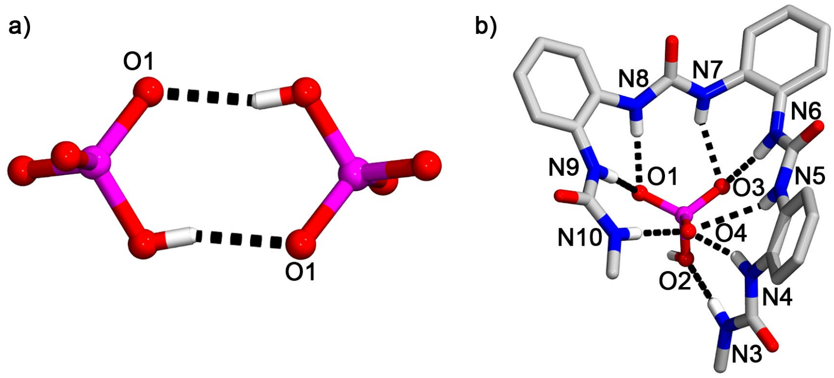

Fig S80. a) the hydrogen bond interaction between HPO_4^{2-} dimer molecules; b) hydrogen bonds formed between a PO_4^{3-} ion and four urea units;

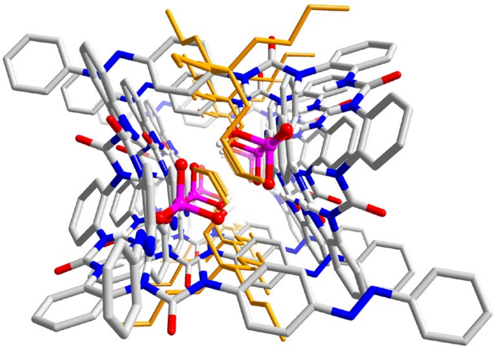

Fig S81. Molecular stacking structure of complex ***EE*-2** along the c-axis in space.

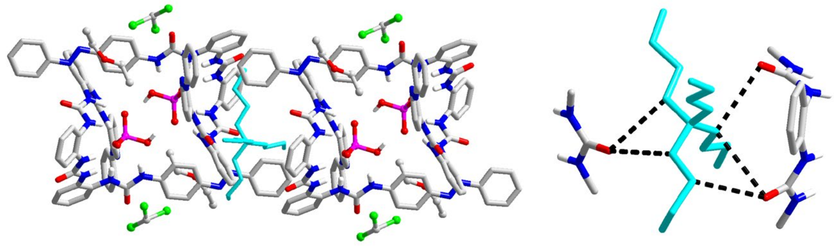

Fig S82. TBA$^+$ cation of outside the pore channel were stabilized through C−H···O non-covalent interactions.

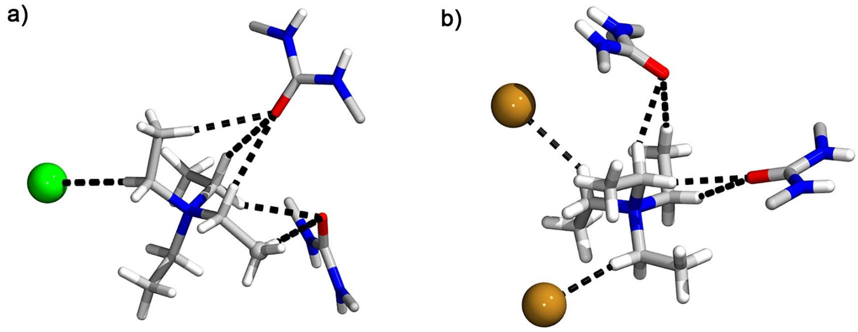

Fig S83. C−H···O and a) C−H···Cl interactions around TPA^+ cation; b) C−H···Br interactions around TBA^+ cation.

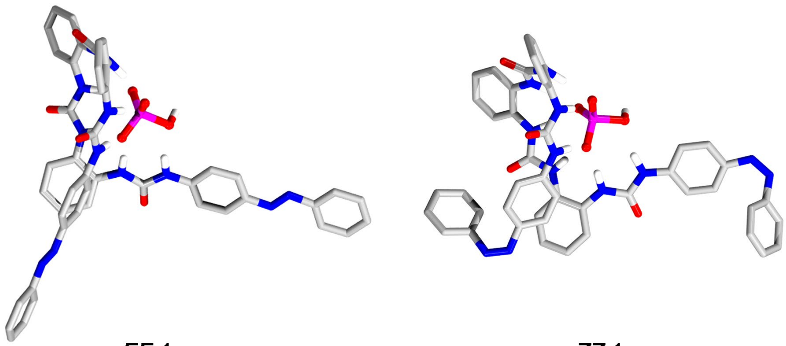

***EE*-1** ***ZZ*-1**

Fig S84. DFT-optimized structures of ***EE*-1** and ***ZZ*-1** with $\mathbf{L^1}$ and HPO_4^{2-}.

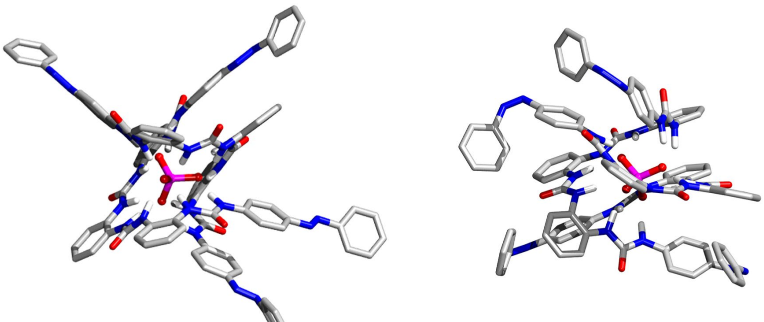

***EE*-3** ***ZZ*-3**

Fig S85. DFT-optimized structures of ***EE*-3** and ***ZZ*-3** with $\mathbf{L^1}$ and PO_4^{3-}.

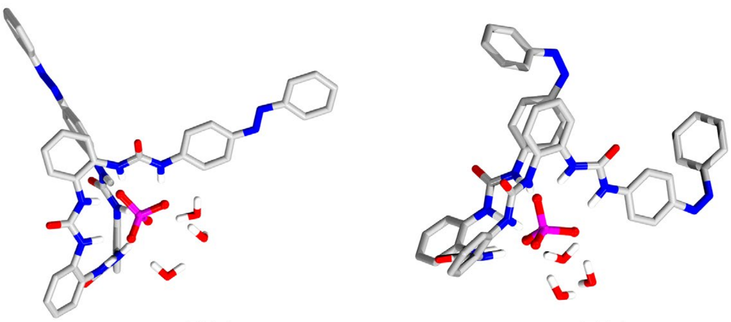

***EE*-4** ***ZZ*-4**

Fig S86. DFT-optimized structures of ***EE*-4** and ***ZZ*-4** with $\mathbf{L^1}$ and PO_4^{3-}.

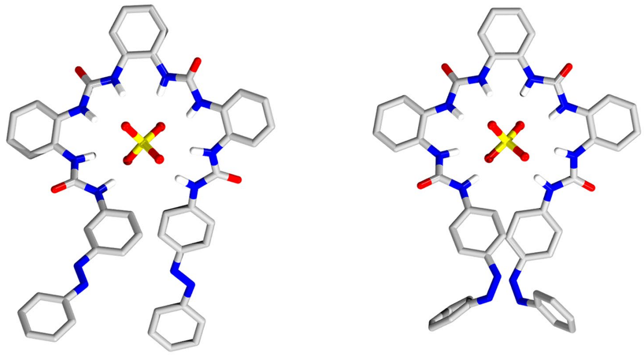

***EE*-5** ***ZZ*-5**

Fig S87. DFT-optimized structures of ***EE*-5** and ***ZZ*-5** with $\mathbf{L^1}$ and SO_4^{2-}.

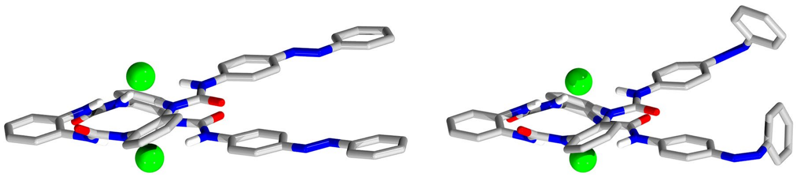

***EE*-6** ***ZZ*-6**

Fig S88. DFT-optimized structures of ***EE*-6** and ***ZZ*-6** with $\mathbf{L^1}$ and Cl^-.

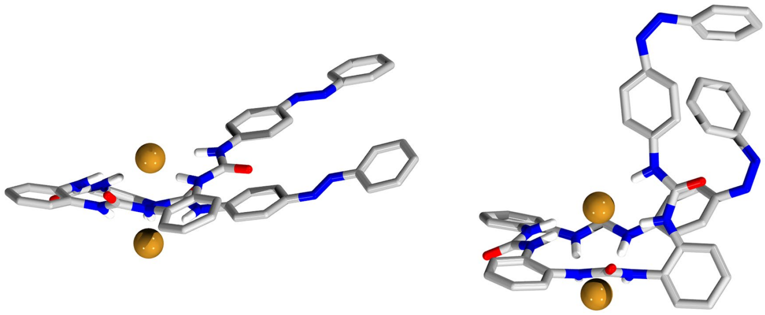

***EE*-7** ***ZZ*-7**

Fig S89. DFT-optimized structures of ***EE*-7** and ***ZZ*-7** with $\mathbf{L^1}$ and Br^-.

Table S1. Distance between two azo group in one side or one ligand (Å)

Species	trans structure	cis structure
$\mathbf{L^1}$	4.00[b]	4.80[b]
$[(PO_4)_1\mathbf{L^1}_2]^{3-}$(**3**)	12.70 [a]	9.45[a]
$[(PO_4)_1\mathbf{L^1}_1\cdot(H_2O)_3]^{3-}$ (**4**)	12.86[b]	10.14[b]
$[(SO_4)_1\mathbf{L^1}_1]^{2-}$ (**5**)	9.05[b]	5.12[b]
$[(Cl)_2\mathbf{L^1}_1]^{2-}$ (**6**)	5.29[b]	5.86[b]
$[(Br)_2\mathbf{L^1}_1]^{2-}$ (**7**)	4.62[b]	8.37[b]

[a] in one side; [b] in one ligand

S9. X-ray crystallography

The diffraction data for complex ***EE*-1**, ***EE*-6** and ***EE*-7** were collected on a Bruker SMART APEX II diffractometer at 150 K or 193 K with graphite-monochromated Mo-K radiation (λ = 1.54178 Å). ***EE*-2** were collected at the BL17B macromolecular crystallography beamline in Shanghai Synchrotron Facility (λ

= 0.72929 Å). An empirical absorption correction using SADABS was applied for all data. The structures ***EE*-1**, ***EE*-2**, ***EE*-6** and ***EE*-7** were solved by the dual methods using the SHELXS program. All non-hydrogen atoms were refined anisotropically by full-matrix least-squares on F^2 by the use of the program SHELXL, and hydrogen atoms were included in idealized positions with thermal parameters equivalent to 1.2 times those of the atom to which they were attached. The crystal data and refinement details are given in Table S2.

CCDC 2482815-2482818 contain the supplementary crystallographic data for this paper. These data can be obtained free of charge from The Cambridge Crystallographic Data Centre via www.ccdc.cam.ac.uk/data_request/cif.

Table S2. Crystal data and refinement details for complexes ***EE*-1**, ***EE*-2**, ***EE*-6** and ***EE*-7**.

	***EE*-1**	***EE*-2**	***EE*-6**	***EE*-7**
Empirical formula	$C_{73}H_{101}N_{14}O_9P$	$C_{83}H_{122}N_{14}O_9PCl_3$	$C_{62}H_{78}N_{14}O_4Cl_2$	$C_{62}H_{78}N_{14}O_4Br_2$
Formula weight	1349.64	1597.26	1154.28	1243.20
Crystal system	Triclinic	Triclinic	Monoclinic	Monoclinic
space group	*P*-1	*P*-1	C_12/c_1	C_12/c_1
a (Å)	13.3324(8)	14.6995(10)	17.970(3	17.912(3)
b (Å)	16.7184(8)	17.2997(12)	19.294(3)	19.276(3)
c (Å)	17.0892(10)	19.5948(13)	9.018(3)	18.977(2)
α (deg)	88.998(2)	112.070(2)	90	90
β (deg)	89.265(2)	98.145(4	106.512(6)	106.345(6)
γ (deg)	76.652(2)	103.745(3)	90	90
V (Å^3)	3705.5(4)	4335.4(5	6321.9(16)	6287.6(15)
T (K)	150	150	193.1	193
Z	2	2	4	4
D_{calc} (g·cm^{-3})	1.210	1.224	1.213	1.313
Total no. of data	65588	43599	23745	28262
No. of unique data	14086	12134	5544	7193
θ range (deg)	1.768-25.757	1.339-23.819	2.214-25.025	1.739-27.529
Completeness to θ	99.7 %	91%	99.2 %	99.9 %
Goodness-of-fit on F^2	0.977	1.071	1.066	1.020
R(int)	0.0538	0.0348	0.0560	0.0785
$R1$ [I>2σ(I)]	0.0981	0.1045	0.1424	0.0541
$wR2$ [I>2σ(I)]	0.2429	0.2989	0.3760	0.1101

Table S3. Hydrogen bonds around the HPO_4^{2-} ions in ***EE*-1**.

D−H···A	d(D−H)	d(H···A)	d(D···A)	∠(DHA)
N8-H8···O1	0.88	2.00	2.856(2)	163
N9-H9···O1	0.88	1.92	2.799(2)	174
N6-H6···O2	0.88	1.80	2.678(2)	173
N7-H7···O2	0.88	2.11	2.862(2)	144
N4-H4···O3	0.88	1.94	2.722(2)	148
N5-H5···O3	0.88	2.40	3.125(2)	140
N10-H10···O3	0.88	1.95	2.791(2)	160
N3-H3···O4	0.88	2.28	2.148(2)	167
O4-H4A···O1	0.84	1.77	2.604(19)	171

Table S4. Hydrogen bonds around the HPO_4^{2-} ions in ***EE*-2**.

D−H···A	d(D−H)	d(H···A)	d(D···A)	∠(DHA)
N8−H8···O1	0.86	1.98	2.830(3)	169
N9−H9···O1	0.86	2.07	2.916(3)	166
N6−H6···O3	0.86	1.86	2.710(3)	173
N7−H7···O3	0.86	2.20	2.863(3)	134
N3−H3···O4	0.86	2.42	3.150(3)	143
N4−H4···O4	0.86	1.88	2.689(3)	157
N5−H5···O4	0.86	2.58	3.291(3)	141
N10−H10···O4	0.86	1.94	2.796(3)	171
O2−H2A···O1	0.82	1.84	2.638(2)	165

Table S5. Hydrogen bonds around the Cl^{-} ions in ***EE*-6**.

D−H···A	d(D−H)	d(H···A)	d(D···A)	∠(DHA)
N3−H3···Cl1	0.88	2.63	3.454(3)	157
N4−H4···Cl1	0.88	2.57	3.410(9)	159
N5−H5···Cl1	0.88	2.71	3.533(9)	155
N6−H6···Cl1	0.88	2.55	3.403(9)	165

Table S6. Hydrogen bonds around the Br^{-} ions in ***EE*-7**.

D−H···A	d(D−H)	d(H···A)	d(D···A)	∠(DHA)
N3−H3···Br1	0.88	2.63	3.454(3)	157
N4−H4···Br1	0.88	2.56	3.400(3)	159
N5−H5···Br1	0.88	2.69	3.508(3)	155
N6−H6···Br1	0.88	2.56	3.390(3)	165

S10. Supporting References

(1) H. Li, L. Kou, L. Liang, B. Li, W. Zhao, X.-J. Yang, B. Wu, Chem. Sci., 13 (2022) 4915-4921.